



MASTER THESIS
修士論文

Observational Studies of Fine Scale Structures in Sunspot Umbrae

黒点暗部微細構造に関する観測的研究

Hiroko WATANABE
渡邊 皓子

*Department of Astronomy, Kyoto University, JAPAN
Kwasan and Hida Observatory, Kyoto University*

January 29, 2009

Acknowledgments

This thesis was completed with invaluable help of many scientists, engineers, and my fellow graduate students.

First, I would like to express my sincere gratitude and appreciation to my supervisor, Dr. R. Kitai. He encouraged me to participate in the *Hinode* data analysis as soon as I started my master's program. The theme attracted me, and he greatly helped me analyze the *Hinode* data. Thanks to his dedication, we could successfully submit a paper to PASJ in June 2007.

Prof. K. Ichimoto, my vice supervisor, taught me many instrumental information about the *Hinode* and the Domeless Solar Telescope. His profound knowledge about sunspots arose my enthusiasm for a research of sunspots.

I would like to thank Prof. K. Shibata for giving me many theoretical insights. He encouraged me to join the scientific operator team as a Chief Observer (CO) of the SOT, which was a valuable experience for me. He has also taught me the importance of presentation for researchers.

I am also grateful to scientists in NAOJ, especially Prof. S. Tsuneta, and Dr. Y. Katsukawa, for their great collaborations and guidances. They invited me occasionally to NAOJ, and had time for many fruitful discussions.

I want to convey my special gratitude to Dr. R. Schlichenmaier and Dr. T. Rimmele. I had the great fortune to talk with them when they came to Japan, and they kindly introduced me the unique usage of IBIS data. I am also grateful to Dr. A. Tritschler, who is one of my co-authors, for the inspiring discussion and assistance.

I wish to acknowledge all the members of Kwasan and Hida Observatories, and my fellow colleagues in Kyoto University. I especially owe much to them for offering me many helpful comments and suggestions, and making my school life enjoyable.

Finally, I would like to express my sincere thanks to my parents and my sister, for their continuous understandings and generous support. Without their support, this work could not have been completed.

This work is financially supported by the Grant-in-Aid for Creative Scientific Research "The Basic Study of Space Weather Prediction" (Head Investigator: K. Shibata) from Ministry of Education, Culture, Sports, Science and Technology (MEXT), Japan, donation from the Sun Microsystems Inc.. I also receive financial support from the Grant-in-Aid for the Global COE Program "The Next Generation of Physics, Spun from Universality and Emergence" from the MEXT of Japan.

Abstract

Sunspots are one of the oldest well-known and at the same time most mysterious scientific objectives in astronomy. A sunspot consists of a dark umbra and an annular penumbra encompassing the umbra. Although sunspots have been observed since the time of Galileo, their basic magnetic character has not been clarified even today. We still lack a thorough understanding of their structure and evolution. Why do sunspots emerge? What's going on below sunspots under the photosphere? What kind of fine structures do exist in sunspots? Why are there penumbrae? ... Many of these thought-provoking problems remain open questions. Moreover, it is only by studying the physics of these sunspots that we shall be able to describe the prominent starspots that appear on other active stars.

One of the reasons why a sunspot remains puzzling is the difficulty of its observation. For a photometric observation, the darkness of sunspots inhibits visualizing fine structures, because of the insufficient photon counts. For a spectroscopic observation, the coolness of sunspots makes spectral fitting complicated, because of the blending of molecular lines. Moreover, it is inevitable for a ground-based observation to be influenced by seeing conditions and limited by daylight hours. For these reasons, we could not get satisfactory data to reveal the whole evolution of sunspots and tiny scale structures in sunspots, such as penumbral filaments, light bridges, and umbral dots (UDs).

UDs are small-sized (~ 300 km) bright points in the umbrae. They are present in all sunspots and pores without any exceptions. No sooner than the first observation of UD by Chevalier (1916), it became apparent that UD play an important role in the energy balance in sunspots. The brightness of an umbra decreases about 20-30% of that of quiet regions, because the convection is suppressed drastically in the presence of a strong magnetic field. However, in order to account for the observed brightness of the sunspot, we can not neglect the convective energy. The heat must be supplied by the convective heating in the umbra: a key indication for this is an UD. The individual UD is small, but collectively the dots occupy the large part of the heat flux through the umbra. The mechanism of UD triggering, along with the modeling of sunspots, is fully controversial even in these days. There are two promising models for the interpretation of UD; one is the "monolithic model" and the other is the "spaghetti model". The monolithic model considers UD as the manifestations of overstable convection in a magnetic plasma (Cowling 1957; Knobloch & Weiss 1984). On the other hand, in the spaghetti model, UD are interpreted as the thermal signature of field-free gas that is pushing magnetic field lines aside and penetrating from below into the photosphere (Parker 1979). Currently, observations do not yet clearly favor either of the two models (Watanabe et al. 2008; Rimmele 1997; Rimmele 2008).

Because UD are a signature of convection, they should interact with the deep convective layers which can never be observed directly. Recently, helioseismological techniques have revealed the subsurface structure of the sun to some extent, but far from completeness. The

study of UDs is another method to obtain subsurface information. Although there are some discrepancies with observations, a few 3D MHD simulations already succeeded in reproducing the whole sunspot structure with a penumbra and UDs. The precisely observed parameters of UDs can be used for confirmation of such kinds of simulations, leading to an improved understanding of magnetoconvection in sunspots, and thus in starspots.

Japan's third solar physics mission, the *Hinode* satellite, made it possible to trace solar fine structures under stable, high-accuracy conditions. The biggest advantage of the *Hinode* is that it is free from atmospheric disturbances. Besides, the *Hinode* is equipped with a large 50 cm aperture optical telescope. I completed three observational studies about UDs by taking full advantage of the *Hinode* data.

The principal subject of this thesis is to investigate the basic structure and evolution of UDs, and to research the relation of UDs to the whole structure of sunspots. This project can be performed best by the *Hinode* data, because we can track individual UDs using the stable high-resolution filtergram data. In addition, we can derive their magnetic nature using the simultaneous high-accuracy spectropolarimetric observations. The first study is a statistical study of UDs by analyzing *Hinode*'s filtergram data (Section 2). Size, lifetime, and proper motion of UDs are reported. These results were published in PASJ *Hinode* Special Issue in Kitai et al. (2007). The second study is to examine the magnetic field character of UDs by using *Hinode*'s spectropolarimetric data (Section 3). We found that the reduced magnetic field, the inclined magnetic orientation, and the local upward velocity show a center-to-limb variation. This result may be explained by the formation height difference, depending on the position of the observed sunspot. Section 3 is based on a paper which was accepted for publication by PASJ (Vol. 61, to be published in April 2009). The third study is devoted to the unique study of the dependence of UD's characteristics on their magnetic nature by using both the filtergram and the spectropolarimetric data. We clarified the dependence of lifetime, size, and occurrence rate of UDs on the configuration of the sunspot, or strength of the magnetic field.

Contents

1	Introduction	6
1.1	Sunspots	8
1.1.1	Penumbra	8
1.1.2	Umbra	11
1.1.3	Pore	12
1.2	The <i>Hinode</i> satellite	12
1.2.1	Overview	12
1.2.2	Solar Optical Telescope	14
1.3	Purpose of this Study	17
2	Statistical Survey of Umbral Dots	21
2.1	Scientific Background	21
2.2	Observation and Data Reduction	21
2.3	Internal Structure of the Umbra	22
2.3.1	Dark Core	22
2.3.2	Diffuse Component	27
2.4	Umbral Dot	27
2.4.1	Size	27
2.4.2	Lifetime	29
2.4.3	Proper Motion	29
2.4.4	Temperature	31
2.4.5	Light Curve	31
2.4.6	Brightness of UDs and their surroundings	31
2.4.7	Fission and Fusion of Dots	31
2.5	Discussion	33
3	Magnetic Structure of Umbral Dots	37
3.1	Scientific Background	37
3.2	Observation	38
3.3	Stokes <i>V</i> area asymmetry	38
3.4	Magnetic Structure and Doppler Velocity Distribution around UDs	39
3.4.1	Inversion	39
3.4.2	Identification of UDs	42
3.4.3	Statistics over three days	42
3.4.4	Center-to-limb variation	43
3.5	Discussion and Summary	47
3.5.1	Fe I formation height	47

<i>CONTENTS</i>	5
3.6 Filling factor	49
3.7 Comparison with sunspot models	49
3.7.1 The monolithic model	49
3.7.2 The field-free intrusion model	50
4 Dependence of Umbral Dots on their Magnetic Nature	54
4.1 Scientific Background	54
4.2 Observation and Data Reduction	54
4.3 Automatic Detection Algorithm	56
4.4 Results	59
4.4.1 Histogram	60
4.4.2 Scatter Diagrams	60
4.4.3 Spatial Distribution	62
4.4.4 Lightcurve	65
4.5 Discussion	68
5 Summary and Future Work	73

1. Introduction

The solar atmosphere is classified roughly into 4 layers; the photosphere, the chromosphere, the transition layer, and the corona. The solar photosphere starts from the height where the optical depth for the continuum wavelength (500nm) becomes unity. With most of the visible light, we can see this photosphere. It emits an almost perfect black body radiation with a surface temperature of 5800K. The chromosphere is a layer which satisfies $dT/dh > 0$ (T : temperature, h : height above the photosphere) located just above the photosphere. As can be seen in Fig. 1.1, the chromosphere covers the height from $h = 600\text{km}$ to 2000km . Isn't it strange that the chromosphere is hotter than the photosphere, despite the fact that the heat source (nuclear fusion) is located in the core of the sun? This mystery is called the "chromospheric heating problem." The chromosphere can be observed clearly through special narrow-band optical filters tuned to the $H\alpha$ line center (656.3nm). The transition layer lies in a narrow region between the chromosphere and the corona. In the transition layer, physical conditions, such as temperature and gas density, change drastically along the height. Many EUV (extreme ultraviolet) emission lines originate from this layer. The corona, the uppermost layer of the atmosphere, offers the most puzzling questions. Why is the corona heated up to 10^6K ? What is the source of this "coronal heating"? It has long been the subject of heated debates, but no one can answer these questions completely at this moment.

In our study, we focus on the photospheric observations, especially on sunspot observations. It is commonly accepted that the magnetic field is one of the most important factors that drives active events in space, such as jets and flares. The sun, the closest star from the earth, causes many magnetic activities, such as sunspots, flares and coronal mass ejections. We can approach the mechanism of such magnetic activities on the sun in best detail! The sun is still the only observable experimental laboratory of magnetic fields in the universe. Sunspots are the most prominent magnetic structures in the sun and have been studied intensively. However, even the formation mechanism of sunspots is not yet understood adequately. Dynamo theory predicts that the magnetic field is created below the photosphere, in the convection zone. The photosphere is the closest layer among the observable solar atmosphere to the assumed formation height of the magnetic field. Hence, the observation of the photosphere is a key to the understanding of the mechanism and dynamics of the solar magnetic field. As the sun is a standard G type star according to the spectral classification, the study of sunspots is not confined to the sun itself, but is open for the application to a great number of stars in the universe.

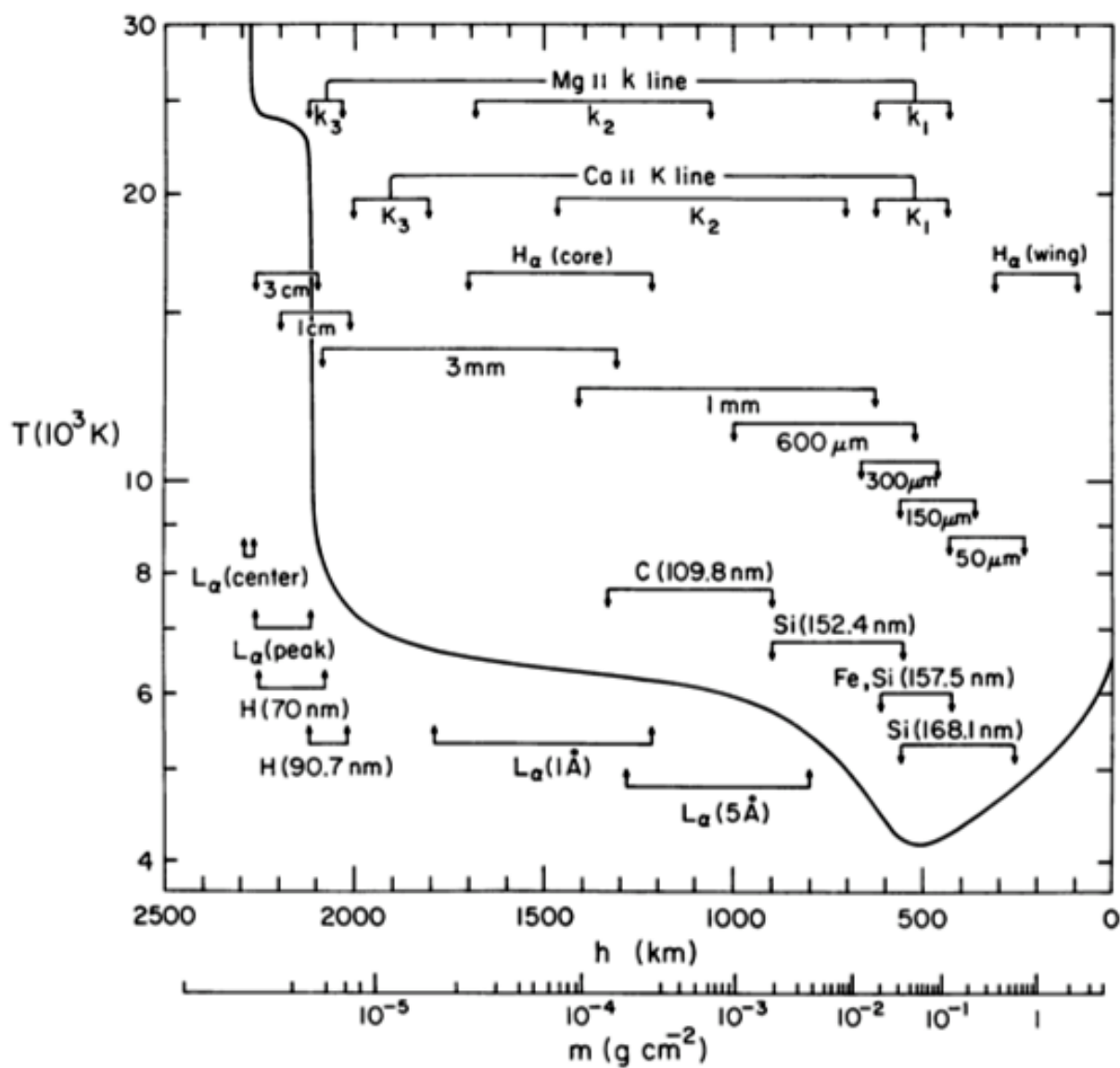


Fig. 1.1.— The average quiet-sun temperature distribution and the regions where various spectral features are formed as a function of height above the photosphere. (Vernazza et al. 1981, Fig. 1)

1.1. Sunspots

Sunspots are one of the most prominent magnetic structures on the solar surface, which are observed as dark in the white light images. There are two components in a sunspot; umbra and penumbra (see Fig. 1.2). The umbra is an extremely dark feature in the center of the sunspot, whose brightness is about 0.3 times that of the quiet region. The penumbra is an aggregation of filamentary structures and encircles the umbra. The penumbra is also dark, but slightly brighter than the umbra, about 0.7-0.8 times as bright as that of the quiet region.

In the early 20th century, two significant progresses were made about sunspots. The first one was the discovery of magnetic fields by Hale. In 1908, Hale discovered that sunspots contain strong magnetic fields by the Zeeman splitting measurement of magnetically sensitive absorption lines. This was the first discovery of an extraterrestrial magnetic field! Recent studies show that the field strength is typically 3000Gauss within an umbra. The second big progress was the discovery of a persistent radial outflow in the penumbra by Evershed in 1909. This outflow is called “Evershed flow”, and its origin is not clear even now. One of the most prevalent theories is that it is driven by the gas pressure difference at the two footpoints of the flux tube (“siphon flow”, Thomas 1988; Degenhardt 1989, 1991).

Recent observations revealed many fine structures in sunspots, as is shown in Fig. 1.3. Bright tiny points, called “umbral dots”, are distributed almost all over the umbra, showing that the umbra is far from being uniform. The penumbra is made of numerous filamentary structures, called “penumbral filaments.” Some sunspots, especially disintegrating ones, are likely to have “light bridges”, which are bright slender structures running across the umbrae.

The fundamental discussion why sunspots look dark was first developed by Biermann and Cowling. Biermann (1941) suggested that, wherever there is a strong magnetic field, the field tries to suppress the convection through braking of the eddy motion. Later on, Cowling (1953) pointed out the possibility that the magnetic field may only reduce (rather than fully suppress) convective heat transport within a sunspot. This kind of discussion has been advanced in recent days, using new helioseismic techniques (Zhao et al. 2001) or realistic 3 dimensional MHD simulations (Rempel et al. 2008). However we have not yet obtained an ultimate model of a sunspot configuration, and there is still an argument whether the basic magnetic field configuration of the sunspot is nonuniform (“spaghetti model”, Parker 1979) or uniform (“monolithic model”, Weiss et al. 2002).

1.1.1. Penumbra

The penumbra shows a highly complex magnetic structure. The inclined and the vertical magnetic fields distribute side by side, and form the “uncombed structure” (Solanki & Montavon 1993; Bellot Rubio et al. 2003). The dark penumbral filaments spatially corre-

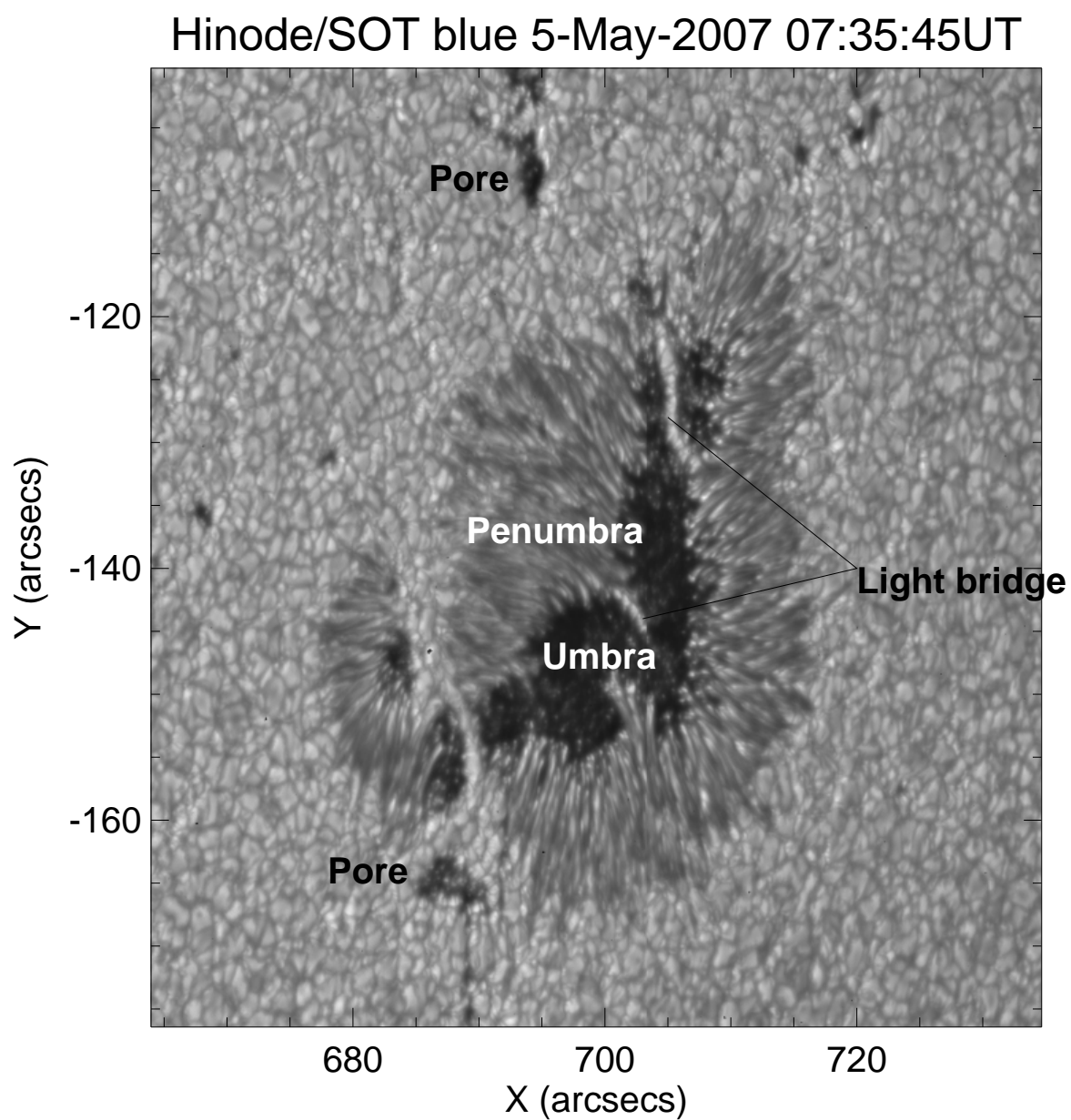


Fig. 1.2.— The magnetic structures on the photosphere seen at the blue continuum wavelength (4505\AA). The active region shown is NOAA 10955. See text for explanations.

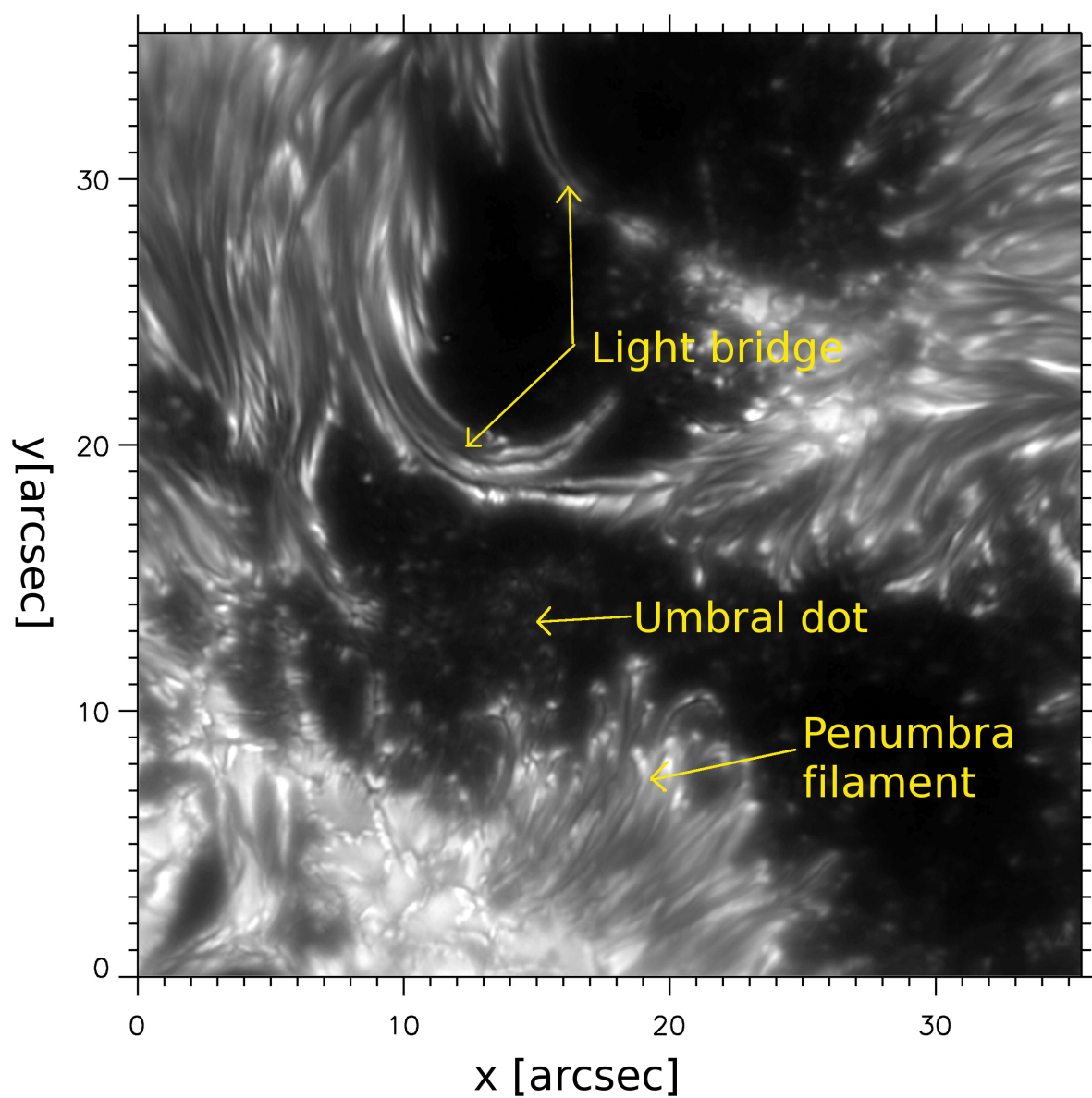


Fig. 1.3.— G-band image of AR 10484, showing sunspot fine structures. This image was taken with Dunn Solar Telescope on October 23, 2003, near the disk center. (Rimmele 2008, Fig. 1)

spond to the inclined magnetic fields, and the bright penumbral filaments correspond to the vertical ones. The most characteristic velocity field seen in the penumbra is the Evershed flow. The Evershed flow is a universal phenomenon observed in all penumbrae, and flows outward from the umbra. The velocity of the Evershed flow reaches almost 6.5 km s^{-1} in the photosphere, which is only slightly smaller than the local sound speed. The Evershed flow is mainly concentrated in dark-cored filaments where the field is weaker and more inclined. Recently, Scharmer et al. (2002) found dark lanes located in the middle of the penumbral filaments from high resolution observations. The inner footpoint of the dark-cored filaments is usually associated with a penumbral bright grain. The penumbral grain moves towards the center of the umbra, and the tips of the penumbral grain that is separated from the filamentary structure is called a peripheral umbral dot.

Many theoretical models were proposed to account for the penumbral structure and associated velocity field, such as the siphon flow model (Thomas 1988), the interchange convection of flux tubes (Schlichenmaier et al. 1998), and the gappy penumbra model (Spruit & Scharmer 2006). The siphon flow model is based on the flow driven by the difference in the gas pressure at the two footpoints of the flux tubes. In the interchange convection model, the inclined magnetic flux tubes evolve dynamically within the penumbra and are able to transport heat more efficiently than magnetoconvection in the umbra. The onset of interchange convection depend on the slope of the magnetic field lines. The gappy penumbra model assumes the penumbra as gappy below the observed surface. The penumbra showing Evershed flow is the convective manifestation occurring in this field-free gaps. Unfortunately, numerical experiments have not yet succeeded in reproducing the stable structure of a real penumbra.

1.1.2. Umbra

As can be seen in Fig. 1.3, the umbra is also far from uniform. Umbral dots (UDs), the main target of our thesis, are tiny bright points in the umbra, and are observed in all of the sunspots without exception. Their size is about 300km and they live about 10 minutes. Light bridges (LBs) have a shape like a bridge spanning the umbra, and are often seen during the disintegrating phase of a sunspot. According to their appearance, LBs are classified into 2 types; photospheric and penumbral types. The photospheric LBs are considered to be an aggregation of granules, while the penumbral LBs are like the extension of the penumbral filaments. There are some especially dark regions which include few UD. They are called “dark cores”. A dark core has a very strong magnetic field in the umbra ($>3000 \text{ Gauss}$), and shows very low temperature about 3500K (cf. the temperature of the quiet region is about 6000K).

The physical mechanism that controls the fine structures in the umbra is considered to be the convection. The umbra has a strong magnetic field of a few thousand Gauss. In

the presence of a strong magnetic field, convection is effectively suppressed. However, small scale convection is occurring and contributes to the energy transportation in the umbra. The signatures of convection are UDs and LBs. The conditions which determine the size and lifetime of UDs and LBs are of considerable interest for the theory of magnetoconvection. The dark core has a very strong magnetic field, and thus include fewer UDs than the other regions in the umbra. UDs and LBs are crucial for our understanding of the subsurface structure of sunspots, which is hidden from direct observations. Moreover, UDs are important for understanding why there is a sharp boundary between an umbra and a penumbra, since part of UDs are the tips of penumbral grains which are detached and migrate inward to the center of the umbra.

1.1.3. Pore

In §1.1, I explained that a sunspot has two structural components, that is, umbra and penumbra. However, on the solar surface, there are dark magnetic features without penumbra. Those are known as pores (see Fig. 1.2). The pores have a simpler structure compared to sunspots, because they do not show a complex penumbra. Moreover, because the pores are thought to be in a developing phase of the evolution from small magnetic features to sunspots, it is important to cover the evolution of their structure. In spite of their importance, there have been only few studies compared to sunspots (Morinaga et al. 2008). Inside the pore, we can see UDs as well as in the sunspot umbra. Studying UDs in pores can reveal information on how UDs are related to the existence of penumbra. Usually, the size of UDs in pores is larger than those in sunspots.

1.2. The *Hinode* satellite

1.2.1. Overview

Japan's third solar physics mission, *Hinode*, was launched on September 23, 2006. *Hinode* has three scientific instruments: Solar Optical Telescope (SOT), Extreme ultra-violet Imaging Spectrometer (EIS), and X-Ray Telescope (XRT), as is shown in Fig. 1.4. SOT has an unprecedented $0.2''$ resolution under seeing-free, stable conditions (Correlation Tracker & Tip-tilt Mirror System; Shimizu et al. 2008), both in filtergram and spectrogram. EIS has a sensitivity ten times as high as the ESA SOHO instrument (Culhane et al. 2007), and XRT has a spatial resolution of three times as high as Yohkoh (Kano et al. 2008). Moreover, the *Hinode* satellite adopts a sun-synchronous polar orbit, allowing to observe the sun continuously.

SOT observes the layers from the photosphere to the chromosphere, EIS focuses especially on the transition layer, and XRT reveals the corona. All three instruments work

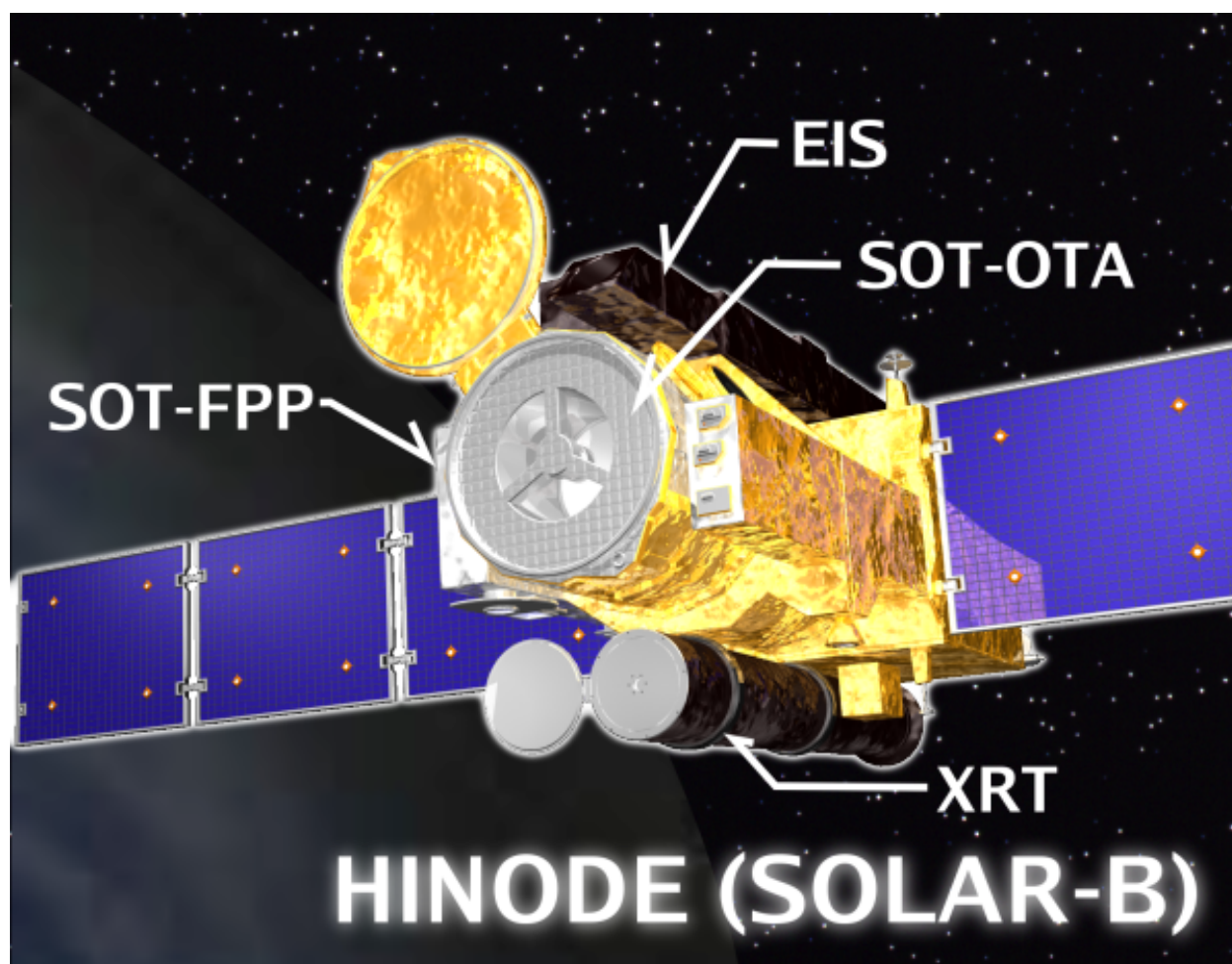


Fig. 1.4.— A cartoon of the *Hinode* satellite. The SOT consists of the main telescope (the Optical Telescope Assembly; SOT-OTA) and the Focal Plane Package (SOT-FPP). The size of the satellite is 4.0m (body length) \times 1.6m (body width) \times 10m (paddle length), and its weight is 900kg. See <http://solar-b.nao.ac.jp/panf/>

complementary to each other, and are aimed to reveal (1) the heating mechanism of the solar corona, (2) the origin of the magnetic field and its dynamics, (3) the basic process in the plasma, such as magnetic reconnection and particle acceleration. The uniqueness of SOT becomes uppermost from its accurate measurement of the vector magnetic field in the photosphere (Ichimoto et al. 2008). A detailed description of SOT will be given in the following section, so I limit myself here to brief explanations of EIS and XRT.

EIS is designed for spectral observation of the transition region. The detector covers the wavelength ranges of 170-210Å and 250-290Å, which covers the regions from the higher chromosphere to the corona. There are two observation modes, slit (1" or 2" width) and slot (40" or 266" width), to be chosen as optimal for the spatial and temporal scales of the target. By investigating emission lines, we can derive the physical parameters such as temperature, gas density, line-of-sight velocity, and so on. Asai et al. (2008) found some blueshifted phenomenon associated with a X class flare. They claimed this to be the first spectroscopic observation of a MHD fast-mode shock associated with a flare.

XRT is equipped with 9 analysis filters to diagnose a wide range of temperatures: thin-beryllium, med-beryllium, thick-beryllium, carbon-poly, thin-aluminum-poly, thin-aluminum-mesh, med-aluminum, thick-aluminum, and titanium-poly. Especially, the thin-aluminum-mesh filter made it possible to diagnose a cool plasma of 1MK, which is beyond the temperature sensitivity of Yohkoh SXT (Savcheva 2008). XRT has a 35cm aperture and can achieve 2" spatial resolution. This advantage in spatial resolution and temperature coverage led to a surprising findings: small X-ray bright points (XBPs) are seen all over the solar surface, which Yohkoh could not resolve (Kotoku et al. 2007; Kariyappa et al. 2008a,b). Another important finding was done by Sakao et al. (2007). They found a continuous plasma outflow at the edge of a solar active region, which may be a source of the solar wind. XRT is looking forward to revealing the physics of solar flares in the forthcoming solar maximum period with its pre-flare buffer system.

1.2.2. Solar Optical Telescope

SOT is the largest optical solar telescope ever sent to space, which has a 50cm aperture mirror. SOT observes the layers from the photosphere to the chromosphere with two powerful instruments. One is the FilterGraph (FG), and the other is the Spectro-Polarimeter (SP).

In FG observation mode, a CCD camera is shared by the Broad-band Filter Imager (BFI) and the Narrow-band Filter Imager (NFI) (Fig. 1.5). BFI has 6 broadband filters which are centered on CN band, Ca II H, G band, blue continuum, green continuum, and red continuum, respectively. BFI images are suitable for the morphological analysis and the tracing of the temporal evolution of small structures. BFI can achieve the best spatial resolution (0.054") among all telescopes on board the *Hinode* satellite. On the other hand, NFI is aimed to obtain the velocity field and the magnetic field by shifting the wavelength

Table 2 SOT/FPP: filter observations.

Broadband Filter Imager (BFI)					
Field of view		218×109 arcsec (full FOV)			
CCD		4K×2K pixel (full FOV), shared with NFI			
Spatial sampling		0.0541 arcsec/pixel (full resolution)			
Spectral coverage					
Center (nm)	Width (nm)	Line of interest	Purpose		
388.35	0.7	CN i	Magnetic network imaging		
396.85	0.3	Ca ii H	Chromospheric heating		
430.50	0.8	Ch i	Magnetic elements		
450.45	0.4		Blue continuum Temperature		
555.05	0.4		Green continuum Temperature		
668.40	0.4		Red continuum Temperature		
Exposure time		0.03–0.8 s (typical)			
Narrowband Filter Imager (NFI)					
Field of view		328×164 arcsec (unvignetted 264×164 arcsec)			
CCD		4K×2K pixel (full FOV), shared with BFI			
Spatial sampling		0.08 arcsec/pixel (full resolution)			
Spectral resolution		0.009 nm (9pm) at 630 nm			
Spectral band (tunable filter)					
Center (nm)	Width (nm)	Lines of interest	g_{eff}	Purpose	
517.2	0.6	Mg ib 517.27	1.75	Chromospheric Dopplergrams and magnetograms	
525.0	0.6	Fe i 524.71 Fe i 525.02 Fe i 525.06	2.00 3.00 1.50	Photospheric magnetograms	
557.6	0.6	Fe i 557.61	0.00	Photospheric dopplergrams	
589.6	0.6	Na D 589.6		Very weak fields (scattering polarization) Chromospheric fields.	
630.2	0.6	Fe i 630.15 Fe i 630.2	1.67 2.5	Photospheric magnetograms	
656.3	0.6	H i 656.28		Chromospheric structure	
Exposure time		0.1–1.6 s (typical)			
Standard observable examples for filter observations					
Filtergram	A signal exposure for each spectral coverage				
	Frame size	4K×2K, 2K×2K, 1K×2K, or 0.5K×2K			
	Summing	1×1 (1K×2K or smaller), 2×2, or 4×4 pixel			
	Readout time	3.4 s (1×1 sum), 1.7 s (2×2), 0.9 s (4×4) Partial readout for faster cadence			
	Reconfigure time	<2.5 s (for changing filter wheels etc)			
Dopplergram	Image of the Doppler shift of a spectral line derived from narrowband filtergrams at several wavelengths				
	Frame size	4K×2K, 2K×2K, 1K×2K, or 0.5K×2K			
	Summing	1×1 (1K×2K or smaller), 2×2, or 4×4 pixel			
	Duration	12.8 s (4 images, 2×2 sum, 0.8 s exposure)			
Longitudinal magnetogram	Stokes VI images converted onboard from narrowband filtergrams				
	Frame size	2K×1K, 1K×2K, or 2K×2K			
	Summing	1×1 (1K×2K or smaller), 2×2, or 4×4 pixel			
	Duration	8 images (4 wavelengths) are taken. 12.8 s for 1K×2K and ~21 s for 2K×2K			
Stokes $IQUV$ (for vector magnetogram)	$IQUV$ images made onboard from narrowband filtergrams at different polarization modulator positions				
	Shuttered exposures	Frame size	4K×2K, 2K×2K, 1K×2K, or 0.5K×2K		
		Summing	1×1(1K×2K or smaller), 2×2, or 4×4 pixel		
	Shutterless exposures	Frame size	Various		
		Summing	1×1, 2×2, or 4×4 pixel		
		Duration	1.6–12.8 s (1–8 waveplate rotations)		

Fig. 1.5.— SOT filter observation overview (Tsuneta et al. 2008, Table 2)

of the observation using the tunable birefringent filter. NFI also has 6 filters; Mg Ib, Na D, H α , and three Fe I lines. Both BFI and NFI can achieve very high cadence (~ 4 s) observations, which allow us to study events that are changing their structure dynamically, such as prominences (Okamoto et al. 2007; Berger et al. 2008) and spicules (De Pontieu et al. 2007).

Table 3 SOT/FPP Spectro-Polarimeter Observations.

Spectro-Polarimeter (SP)		
Field of view along slit	163.84 arcs (NS direction)	
Spatial scan range	327.62 arcs (transverse to slit, EW direction)	
Spatial sampling (slit)	0.16 arcsec	
Spectral line and coverage	Fe I 630.15 nm Fe I 630.2 nm Coverage: 630.08 nm to 630.32 nm	
Spectral resolution/sampling	3pm / 2.15pm	
Measurement of polarization	Stokes I , Q , U , V simultaneously with dual beam (orthogonal linear components)	
Polarization signal to noise	10^3 (normal map)	
Standard observable (mapping mode) examples for SP		
Normal mapping	Time per position	4.8 s (3 rotations of waveplate)
	Polarimetric accuracy	0.001
	FOV along slit	164 arcsec
	Sampling along slit	0.16 arcsec
	Data size	918K pixels in 4.8 s or 191K pixel s $^{-1}$
	Slit-scan sampling	0.16 arcsec
	Time for map area	50 s for 1.6 arcsec wide 83 min for 160 arcsec wide
Fast mapping	Time per position	One rotation for the 1st slit position and another rotation for the 2nd slit position to form one slit data
	FOV along slit	164 arcsec
	Sampling along slit	0.32 arcsec
	Data size	459K pixels in 3.6 s or 127K pixel s $^{-1}$
	Slit-scan sampling	0.32 arcsec
	Time for map area	18 s for 1.6 arcsec wide 30 min for 160 arcsec wide
Dynamics	Time per position	1.6 s (one rotation)
	FOV along slit	32 arcsec (to reduce data size)
	Sampling along slit	0.16 arcsec
	Data size	179K pixels in 1.6 s or 120K pixel s $^{-1}$
	Slit-scan sampling	0.16 arcsec
	Time for map area	18 s for 1.6 arcsec wide

Fig. 1.6.— SP observation overview (Tsuneta et al. 2008, Table 3)

The SP obtains the full Stokes parameters using the Fe I 630nm absorption line with a polarization accuracy of 0.1%. The spectral field-of-view (FOV) covers two strong magnetic sensitive lines, i.e., Fe I 630.15nm ($g_{\text{eff}} = 1.66$) and Fe I 630.25nm ($g = 2.5$). If we assume a certain atmospheric model which is necessary for the inversion of the Stokes profiles, we can extract the physical parameters such as three dimensional magnetic field components, line-of-sight velocity, temperature, source function, filling factor, and so on. There are three observing modes for the SP from which we can choose depending on our scientific interests. Figure 1.6 summarizes those SP observing modes. Normal map mode takes the longest time for one scan, but boasts the best signal-to-noise ratio.

FG and SP observations can be performed simultaneously, and this function greatly extends the usability and flexibility of SOT data. For example, Katsukawa et al. (2007) revealed the formation process of a light bridge, using high-cadence BFI continuum images for tracing the elongation of a light bridge, and several SP data sets for detecting the corresponding variations of magnetic conditions. The most important and difficult task for observers is to clarify what is the best observing method (filters, time cadence, FOV, timing of SP, ...) for studying the physics of a specific scientific target.

Hinode is a Japanese mission developed and launched by ISAS/JAXA, with NAOJ as domestic partner and NASA and STFC (UK) as international partners. It is operated by these agencies in co-operation with ESA and NSC (Norway).

1.3. Purpose of this Study

Several tens of papers have been published about the observational and theoretical aspects of UDs. The first observation of UDs was achieved by Chevalier (1916). As even the largest UDs were smaller than the observational spatial resolution in those days, it was difficult to determine their sizes. Beckers and Schröter (1968) concluded the UD's diameter of 150-200 km from the measurements of the color index. The determination of the UD's lifetime was much more difficult, because UDs were empirically known to occur successively at almost the same location. Danielson (1964), based on the balloon-borne observation, estimated the averaged lifetime as about 30 minutes, which was longer than the typical lifetime of granules (10 minutes). Kitai (1986) was the first to estimate the proper motion of UDs, and found two types of them: immobile UDs located in the central part of the umbra, and mobile UDs in the peripheral region of the umbra. However, for ground-based observations, the atmospheric seeing prevents achieving a sufficiently high spatial resolution and a stable image quality. So, the satellite Solar Optical Telescope is essential to infer the conclusive information on UDs. Theoretical studies, on the other hand, have made great progress in recent years (Schüssler & Vögler 2006; Rimmele et al. 2008). They succeeded in reproducing UDs in 3D MHD simulations, though there rest a few disagreements with real observations. We are now in such a phase that the space-borne observations allow a judgement about the validity of these simulations.

The main purpose of this thesis is to provide an overall observational understanding of UDs. For a fully reliable determination of the UD's size, lifetime, and proper motion, we submitted a proposal for a sunspot observation with the high spatial and temporal resolutional filtergraph (blue and green continuum) no sooner than the launch of the *Hinode*. In addition, we could perform a unique study of the UD's temperature from taking two color images. Because UDs are undoubtedly magnetic-driven features, the spectro-polarimetric observation also has great significance. With the advent of SP aboard the *Hinode* satellite,

it became possible to achieve a high spatial resolution of $0.3''$, compared to the $1''$ spatial resolution of the Advanced Stokes Polarimeter (ASP; Elmore et al. 1992). The thorough measurement of changes of the magnetic field around UDs leads to a realistic physical picture of UDs. Finally, the combination of the imaging and spectro-polarimetric data allows for an analysis hitherto impossible: we can relate the characteristics of UDs to the local and global magnetic field nature. These results should be explained by existing theories of sunspot and magnetoconvection. Moreover, the study of UDs finally leads to the understanding of the subsurface structure of the sun and, more generally, of stars.

In the following sections, we show the results of analysis of the *Hinode* SOT data. In §2, we statistically study the structure and the evolution of UDs by taking advantage of the continuous observations from space. We derived the UD parameters of size, lifetime, proper motion, temperature, and morphological evolution. The size and lifetime are shown to have the median values of 280 km and 15 minutes, respectively. The proper motion of the penumbra-origin UDs is an umbra-inward flow with the velocity of $\sim 1.0 \text{ km s}^{-1}$. In §3, we focus on the magnetic structures and the Doppler fields of UDs based on the Milne-Eddington inversion of the two iron absorption lines at 6302\AA . The histograms of the magnetic field strength, the inclination angle, and the Doppler velocity of UDs showed a center-to-limb variation; observed at disk center, UDs had (i)slightly smaller field strength ($\Delta B = -17$ Gauss) and (ii)relative blue shifts ($\Delta v = 28 \text{ m s}^{-1}$) compared to their surroundings. When the sunspot got close to the limb, UDs and their surroundings showed almost no difference in the magnetic and the Doppler values. This result supports the picture of the penetration of the weakly magnetized hot gas into a cusp-shaped magnetic field. In addition, some UDs showed the oscillatory lightcurves with multiple peaks separated around 10 min, which may indicate the presence of the oscillatory convection. In §4, we describe a comprehensive study of the UD's characteristics dependence on their magnetic nature. The UDs in the strong magnetic field regions have relatively small size and short lifetime. The velocity of UDs are confirmed to be strongly correlated to the bent angle of the magnetic field, as suggested by the gappy model (Heinemann et al. 2007). Finally in §5, the summary and the future visions are presented.

REFERENCES

- Asai, A., Hara, H., Watanabe, T., 2008, *ApJ*, 685, 622
- Bellot Rubio, L. R., Balthasar, H., Collados, M. & Schlichenmaier, R., 2003, *A&A*, 403, L47
- Berger, T. E., Shine, R. A., Slater, G. L., et al. 2008, *ApJ*, 676, L89
- Biermann, L., 1941, *Vierteljahrsschr. Astr. Gesellsch.*, 76, 194

- Chevalier, S., 1916, *Ann. Obs. Astron, Zo-Sè*, 9, B1
- Cowling, T. G., 1957, *Magnetohydrodynamics* (New York: Interscience)
- Cowling, T. G., in G. P. Kuiper (ed.), *The Sun*, University of Chicago Press, 565
- Culhane, J. L., Harra, L. K., James, A. M., et al. 2007, *Sol. Phys.*, 243, 19
- Danielson, R. E. 1964, *ApJ*, 139, 45
- Degenhardt, D. 1989, *A&A*, 222, 297
- Degenhardt, D. 1991, *A&A*, 248, 637
- De Pontieu, B., McIntosh, S., Hansteen, V. H., et al. 2007, *PASJ*, 59, 655
- Elmore, D. F., Lites, B. W., Tomczyk, S., et al. 1992, *Proc. SPIE*, 1746, 22
- Hale, G. E. 1908, *ApJ*, 28, 315
- Ichimoto, K., Lites, B., Elmore, D., et al. 2008, *Sol. Phys.*, 249, 233
- Kano, R., Sakao, T., Hara, H., et al. 2008, *Sol. Phys.*, 249, 263
- Kariyappa, R. & Varghese, B. A. 2008, *A&A*, 485, 289
- Kariyappa, R. 2008, *A&A*, 488, 297
- Katsukawa, Y., Yokoyama, T., Berger, T. E., et al. 2007, *PASJ*, 59, 577
- Kitai, R., 1986, *Sol. Phys.*, 104, 287
- Kotoku, J., Kano, R., Tsuneta, S., et al. 2007, *PASJ*, 59, 735
- Knobloch, E., & Weiss, N. O., 1984, *MNRAS*, 207, 203
- Morinaga, S., Nagata, S., Ichimoto, K., et al. 2007, *PASJ*, 59, S613
- Okamoto, T. J., Tsuneta, S., Berger, T. E., et al. 2007, *Science*, 318, 1577
- Parker, E. N., 1979, *ApJ*, 234, 333
- Rempel, M., Schüssler, M., & Knölker, M., 2008, *ApJ*, in press
- Rimmele, T. 1997, *ApJ*, 490, 458
- Rimmele, T. 2008, *ApJ*, 672, 684

- Sakao, R., Kano, R., Narukage, N., et al. 2007, *Science*, 318, 1585
- Savcheva, A., 2008, *Proc. IAU*, 247, 326
- Scharmer, G., Gudiksen, B. V., Kiselman, D., et al. 2002, *Nature*, 420, 151
- Schlichenmaier, R., Jahn, K., & Schmidt, H. U., 1998, *A&A*, 337, 897
- Schüssler, M., & Vögler, A. 2006, *ApJ*, 641L, 73S
- Shimizu, T., Nagata, S., Tsuneta, S., et al. 2008, *Sol. Phys.*, 249, 221
- Solanki, S. K., & Montavon, C. A. P., 1993, *A&A*, 275, 283S
- Spruit, H. C. & Scharmer, G. B., 2006, *A&A*, 447, 343
- Thomas, J. H. 1988, *ApJ*, 333, 407
- Thomas, J. H, & Weiss, N. O., 1992, *Sunspots: Theory and Observations*
(Nato Science Series Series C: Mathematical and Physical Sciences)
- Tsuneta, S., Ichimoto, K., Katsukawa, Y., et al. 2008, *Sol. Phys.*, 249, 167
- Vernazza, J. E., Avrett, E. H., & Loeser, R. 1981, *ApJS*, 45, 635
- Weiss, N. O., Proctor, M. R. E., & Brownjohn, D. P., 2002, *MNRAS*, 337, 293
- Zhao, J., Kosovichev, A. G., & Duvall Jr., T. L., 2001, *ApJ*, 557, 384
-

2. Statistical Survey of Umbral Dots ¹

2.1. Scientific Background

Umbral fine structures in sunspots have been studied by many authors. Recent reviews were given in Thomas & Weiss (2004) and in references cited therein. The study of umbral fine features is essential for our understanding of the magnetoconvection in a strong magnetic field atmosphere of celestial bodies. As the spatial size of the umbral fine structure, such as umbral dots (UDs), is very fine, it is challenging to infer the basic characteristics of them. Especially, it was difficult to follow the temporal evolution of the fine features from ground-based telescopes, due to the influences of variable atmospheric seeing conditions.

Solar Optical Telescope (SOT) on board *Hinode*, which was successfully launched on September 23, 2006, was designed to observe the solar fine structure with a 50cm mirror from space (Kosugi et al. 2007). The resolving power in flight condition was confirmed to be nearly the theoretical one of $0.2''$. Using the *Hinode*/SOT, we observed the temporal evolution of umbral fine structures during the period of March 2-4, 2007. Spatial distributions of umbral structures, their temporal evolution, lifetimes, proper motions, temperatures were studied by use of the three days's data set. Besides the basic characteristics stated above, we could follow temporal evolution of fission and fusion events of UD. In the following sections, we describe the details of observation and analysis procedures in §2.2, present our results in §2.3 and §2.4, and finally discuss and summarize our findings in §2.5.

2.2. Observation and Data Reduction

We observed a roundish sunspot in the active region NOAA10944 from March 2 through March 4, 2007. The region was fairly inactive during the three days period and disintegrated on March 5. The region, observed in $H\alpha$ with the Domeless Solar Telescope (DST) at Hida Observatory, is shown in Fig. 2.1. The main sunspot remained as α type during the three days. Among the data taken with the *Hinode*/SOT, we report the results obtained from time-series imaging observation by the Broadband Filter Imager (BFI), shown in Table 2.1. The continuum images were taken through two filters, green ($\lambda = 5550\text{\AA}$, $\Delta\lambda \simeq 5\text{\AA}$) and blue ($\lambda = 4504\text{\AA}$, $\Delta\lambda \simeq 5\text{\AA}$). Both continuum images were taken in a cadence of 1frame/30s. The pixel resolution of the images was $0.054''$. The field of view (FOV) of the continuum images was $55.8'' \times 55.8''$. To follow the temporal evolution correctly without projection effects, we transformed all the images as if they are seen from the top. The daily evolution of the umbral region in green continuum is shown in Fig. 2.2.

¹This chapter is based on a paper published in PASJ, 59, S585-S591, 2007, entitled "Umbral Fine Structures in Sunspots Observed with *Hinode* Solar Optical Telescope"

We applied a median filter (window: $1'' \times 1''$) to all images to identify slowly varying features, such as the dark core area and diffuse components. The effect of median filter processing on the structure identification is shown in Fig. 2.3. All the images were co-aligned by finding image displacements which gives the maximum correlation between consecutive frames.

Temperatures of umbral features were estimated from color values, i.e., the intensity ratio $I(\text{blue})/I(\text{green})$. Therefore, we can measure the temperature only from the data set of March 4. The relation between the intensity ratio and temperature was calculated assuming the black body radiation. The temperature distribution over the region is shown in Fig. 2.4. The temperatures of normal granules surrounding the spot are $\simeq 6000\text{K}$, while those of intergranular lanes are $\simeq 5000\text{K}$. These temperature values are consistent with those known previously.

2.3. Internal Structure of the Umbra

As shown in Fig. 2.2, the brightness distribution of the umbral area is not uniform. The umbra observed by us consisted of a dark core region, diffuse components and bright UDs, as it was observed in previous ground-based works under superb atmospheric conditions (Thomas & Weiss 2004). In our observation, the dark core almost kept its location and size, while the spot gradually evolved and deformed during the three days period. In the dark core, UDs were very scarcely detected. Diffuse components were observed to stay at nearly the same location and develop into light bridges. UDs were numerously detected to appear and disappear, except in the dark core region. The characteristics of individual components are studied separately in the following subsections.

2.3.1. Dark Core

The daily evolution of the umbral dark core is shown in Fig. 2.5. The dark core is located at $(x=68'', y=13'')$ on March 2, $(x=73'', y=2'')$ on March 3, and $(x=88'', y=-10'')$ on March 4. The temperature of the dark core is around 3850K on March 4. As the con-

Table 2.1: Observation information

Date	Time	Filter
2007 March 2	00:14-03:15 UT	green continuum
2007 March 3	00:10-03:30 UT	green continuum
2007 March 4	00:15-03:05 UT	green and blue continua

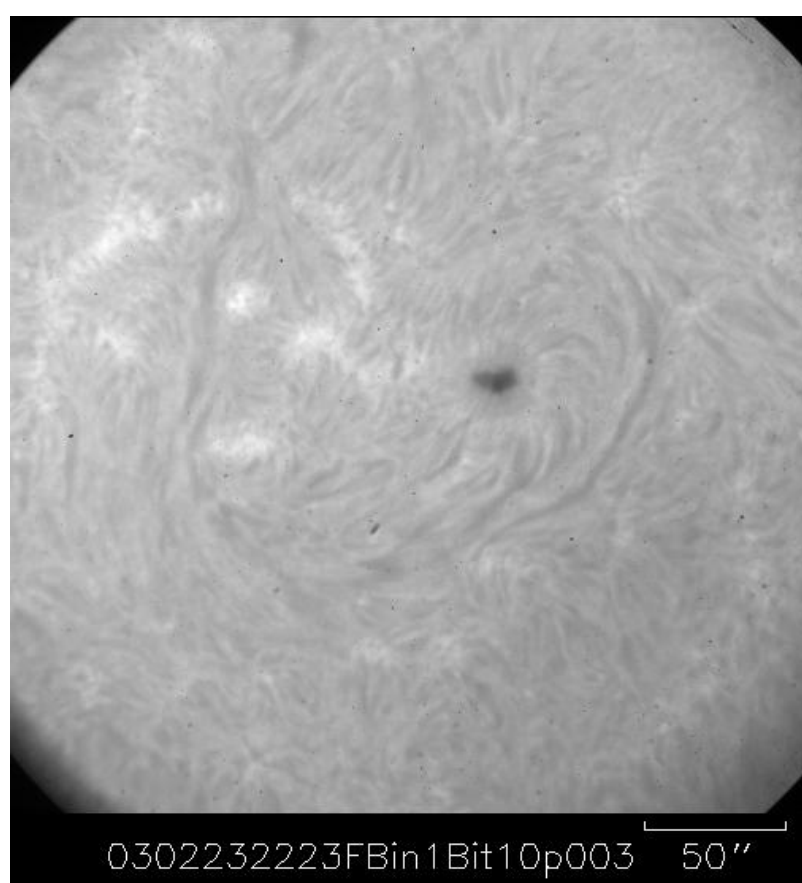


Fig. 2.1.— $H\alpha$ image of NOAA10944 on March 2, 2007, taken by DST at Hida Observatory.

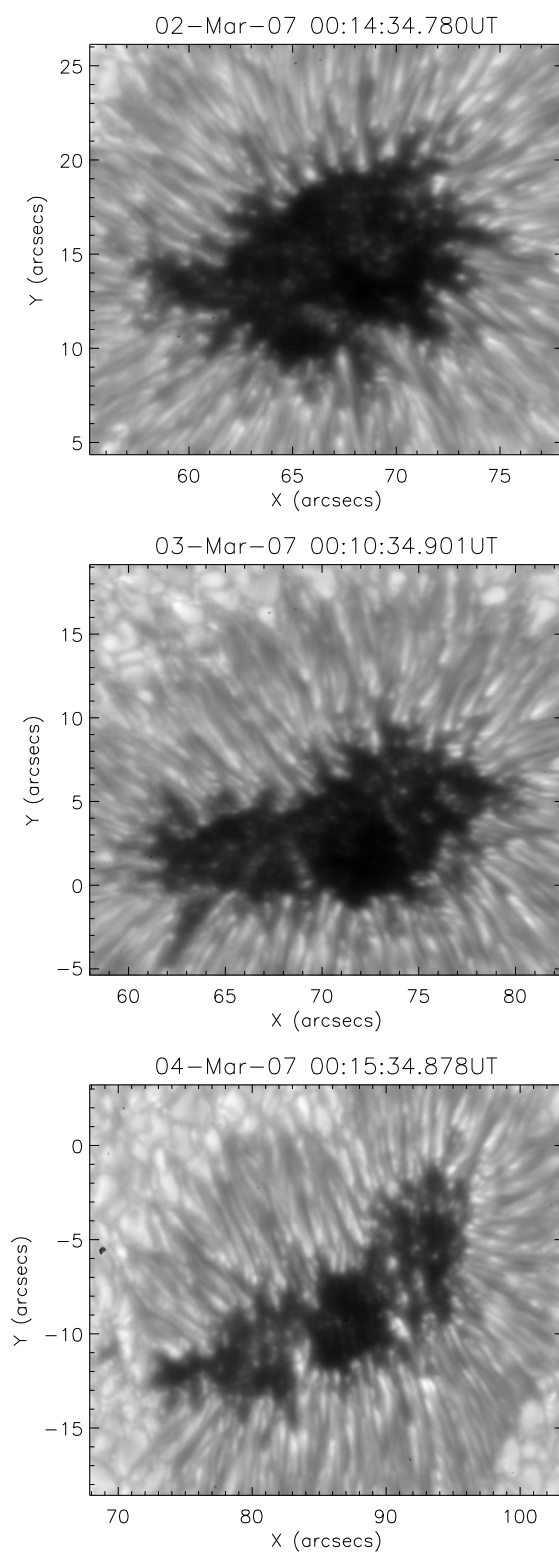


Fig. 2.2.— Daily evolution of the sunspot in green continuum.

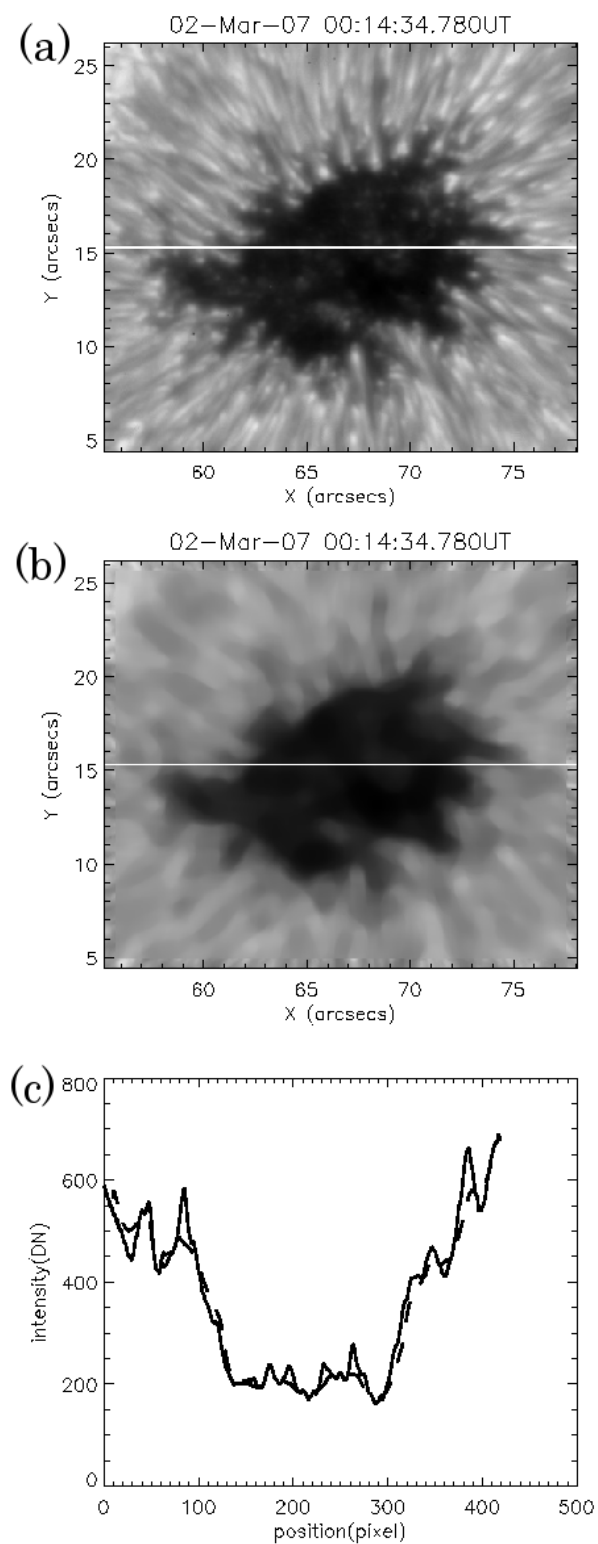


Fig. 2.3.— Effect of median filter. (a) Original image. (b) Filtered image. (c) Intensity plot along the white line indicated in (a) and (b). Both intensity profiles of the original image (solid) and of the median-filtered one (dashed) are shown.

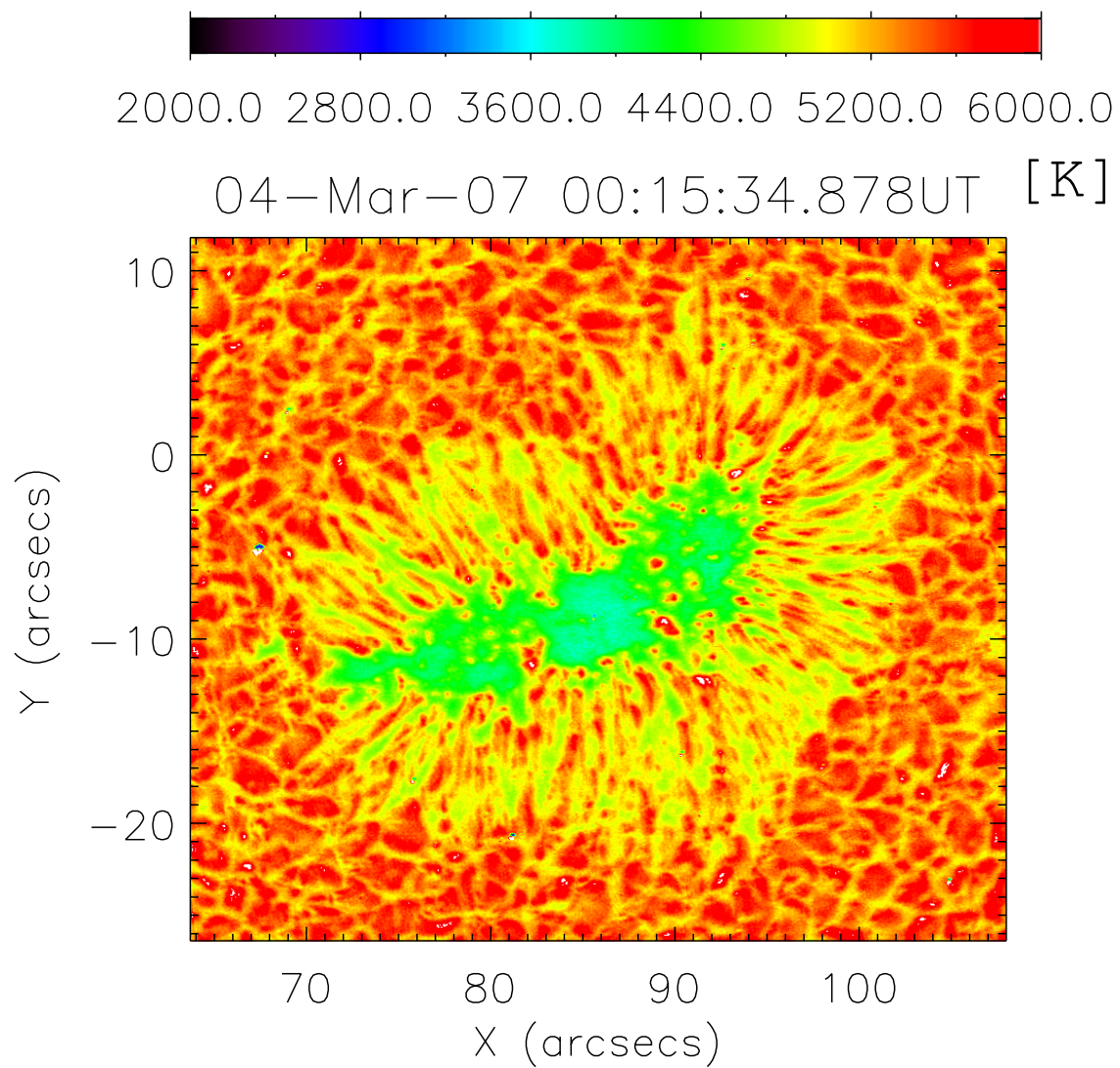


Fig. 2.4.— Temperature distribution on March 4, 2007.

tinuum brightness gradually increased, the core's temperature is expected to have increased with time. This tendency seems to be natural, as the spot was in a decaying phase. We could identify virtually no UDs in the dark core. The absence or very low brightness of UDs in dark cores is confirmed in our observation from space, without the ambiguity of seeing conditions in ground-based observations. This absence is probably due to the positive correlation between the UD's brightness and the background brightness, as stated in §2.4.6.

2.3.2. Diffuse Component

In Fig. 2.5, we see the daily evolution of the diffuse components. On March 2, the region around $(x=67'', y=12'')$ appeared bright compared to the other umbral region, and this region developed to the light bridge seen on March 4, at $(x=84'', y=-11'')$. The same change took place in the region around $(x=68'', y=17'')$ on March 2, which developed to the second light bridge at $(x=91'', y=-6'')$. Their locations were rather stable during the three days. Their brightness increased along time. Temperatures ranged from 4250K to 4500K on March 4, which was 500K hotter than the dark core. They finally took the form of light bridges. In our case, the light bridges were of umbral type, neither of penumbral nor of photospheric type, so the fine structures in the diffuse components had forms similar to UDs (Muller 1979).

2.4. Umbral Dot

As reported in many works (Kitai 1986; Sobotka et al. 1997a; Thomas & Weiss 2004), UDs are usually classified into two classes, i.e., (1) central or umbral origin, and (2) peripheral or penumbral origin. UDs of the former type appear and disappear in central parts of the umbra. Their proper motions are known to be small. On the other hand, UDs of the latter type originate in the penumbral area. Tips of inner penumbral filaments start to be separated and move into the umbral area with a larger velocity than the former type (Kitai 1986). In our present study, we identified about 100 UDs during the three days period. We classified them, like in previous works, into three classes according to their creation, i.e., umbral origin (UUDs), penumbral origin (PUDs) and light-bridge origin (LUDs).

2.4.1. Size

UDs generally have circular shapes. We measured the sizes of them by fitting their spatial profile with a gaussian distribution function. The definition of the size is the average of two FWHMs of the gaussian fit to the horizontal and vertical spatial profiles. The histogram is shown in Fig. 2.6. Our result shows that the sizes of the majority of the UDs, regardless

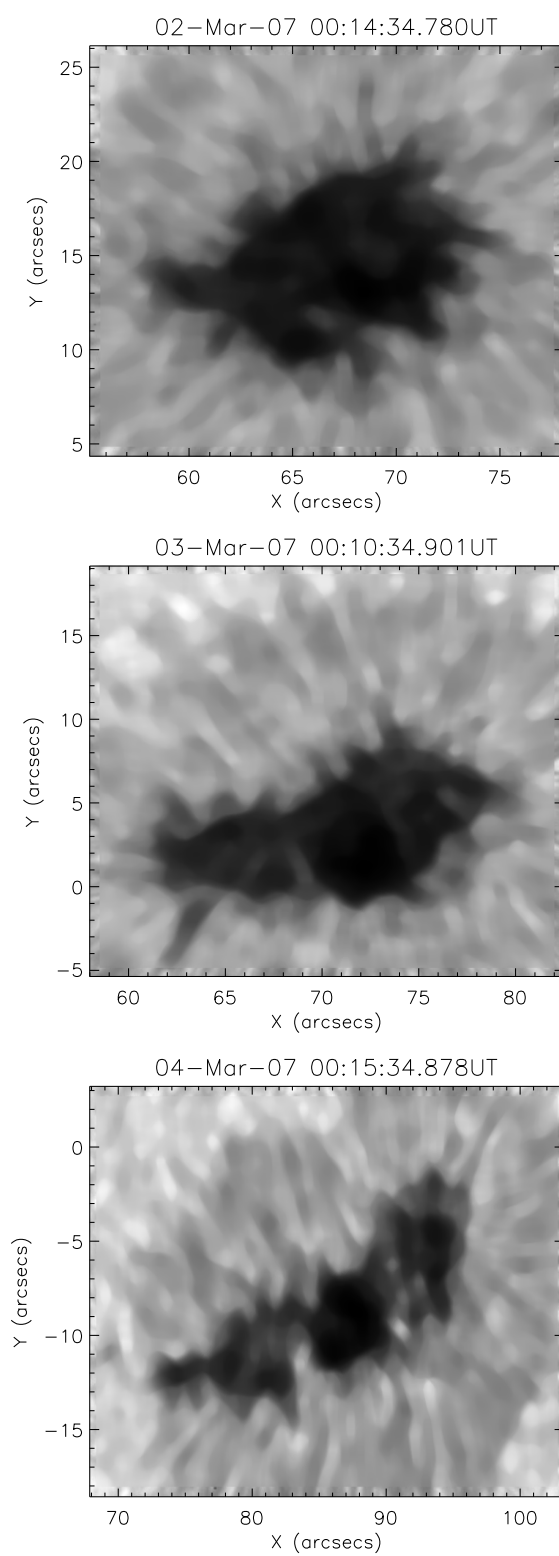


Fig. 2.5.— Daily evolution of the dark core and the diffuse components in green continuum. Median-filtered images are shown.

of the type (UUD, LUD, PUD), are distributed from 200km to 400km. The median value is 280km. However, several percent of the UDs have linear sizes of 150km, i.e., the theoretical resolution limit of the telescope. We should bear in mind that even smaller UDs can exist in umbrae.

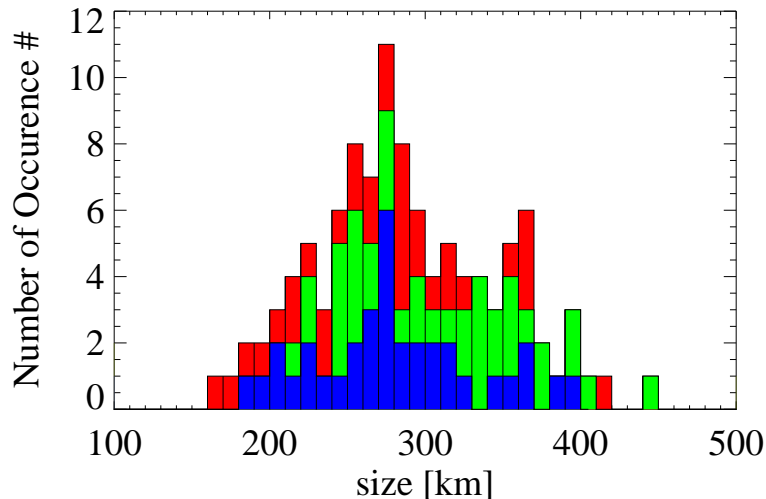


Fig. 2.6.— Histogram of the UD's size distribution. Blue means UUDs, green means LUDs, and red means PUDs. The resolution limit of the *Hinode* FG is 150km.

2.4.2. Lifetime

The lifetime of each UD is determined by the FWHM of the gaussian fit to its light curve after subtracting by the local background intensity (Fig. 2.7). It sometimes occurs that an UD repeatedly appear at the same position. In this case, we divided the light curve into multiple parts with individual peak brightness. As is seen in Fig. 2.8, the lifetime distribution of UUDs and PUDs is similar, with a median lifetime of 14.5 min. On the other hand, the lifetime of LUDs is a bit longer than that of UUDs and PUDs. The median lifetime of LUDs is 19.5 min.

2.4.3. Proper Motion

Proper motions of UDs were derived by tracking the identified features along the time series of the images. The identification of features was achieved visually on the screen. The proper motions of both UUDs and LUDs showed similar behavior. Their velocities are virtually zero, 0.5km s^{-1} at maximum, with random directions of motion. On the other

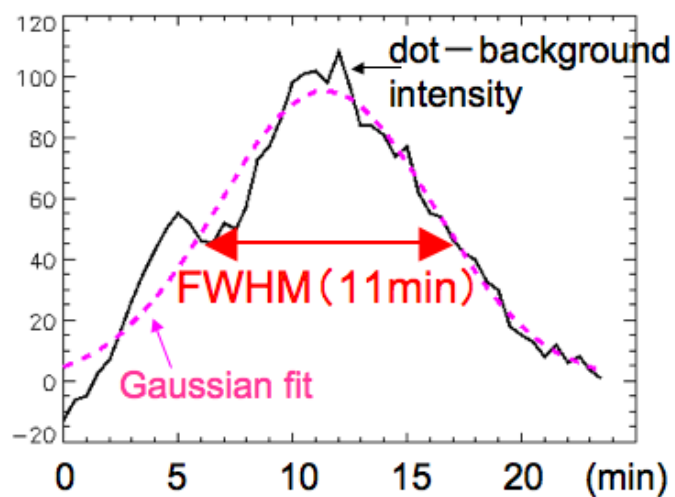


Fig. 2.7.— Definition of the UD's lifetime is shown.

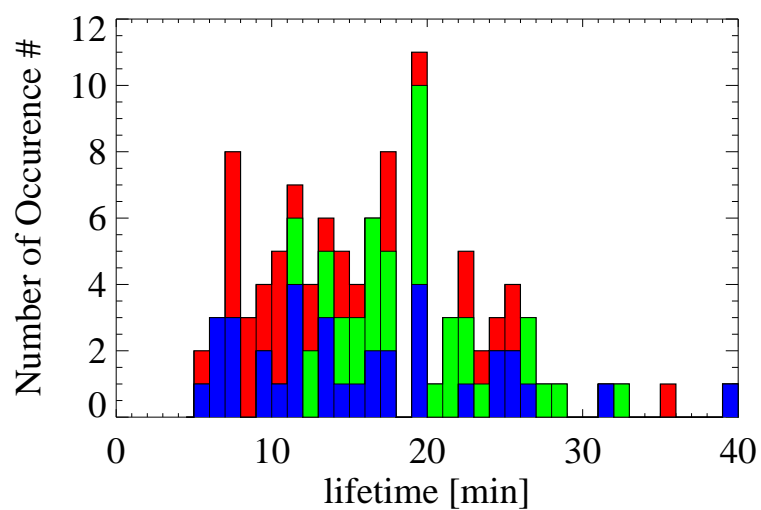


Fig. 2.8.— Histogram of the UD's lifetime distribution. Blue means UUDs, green means LUDs, and red means PUDs. The time cadence of our data set is 30sec.

hand, PUDs showed higher velocities of about 0.9km s^{-1} at their creation and gradually slowed down to 0.5km s^{-1} .

2.4.4. Temperature

The temperatures of UUDs range from 4200K to 5500K of their average being 4600K. Those of LUDs range from 4800K to 5600K with an average of 5100K. PUDs are generally hotter at the time of creation and cool down gradually. Their temperatures range from 4700K to 5900K, and their average is 5460K.

2.4.5. Light Curve

The temporal variation of the brightness is found to depend on the type of UDs. UUDs and LUDs increase their brightness linearly, and then darken linearly with time. The light curve of a long-lived UUD/LUD is shown in Fig. 2.9(a). Contrarily, PUDs darken continuously without increasing their brightness (Fig. 2.9(b)).

2.4.6. Brightness of UDs and their surroundings

The brightness of UDs depends on their surroundings. UDs seen in brighter background appear brighter/hotter than those in dark regions. The correlation between the peak brightness of UDs and their background brightness is shown in Fig. 2.10. From our temperature analysis, UDs are found to be around 300K hotter than their surroundings, irrespective of the type of UDs. This relation was first reported by Sobotka et al. (1992a), and has been studied by Sobotka et al. (1992b, 1993) and recently by Sobotka & Hanslmeier (2005). The analysis of the blue/green continuum brightness from our observation from space with $0.24''$ resolution fully confirms their results.

2.4.7. Fission and Fusion of Dots

Some of UUDs and LUDs show fission and fusion, while majority of UDs keep their identities during their lives. One fission events were observed in the sample of 30 UUDs, while one fission and two fusion events were detected in the sample of 31 LUDs. Sobotka et al. (1997a) noticed these events while tracking the evolution of UDs. Temporal behaviors of fission and fusion are shown in Fig. 2.11. Fissions occurred at the end of UDs's life. They disintegrated into a smaller parts and faded away. Furthermore, two UDs merged into one and form a bright UD when fusion of UDs occurred. For the PUDs, we have not detected these phenomena. The detailed evolution of the events was first observed in our work.

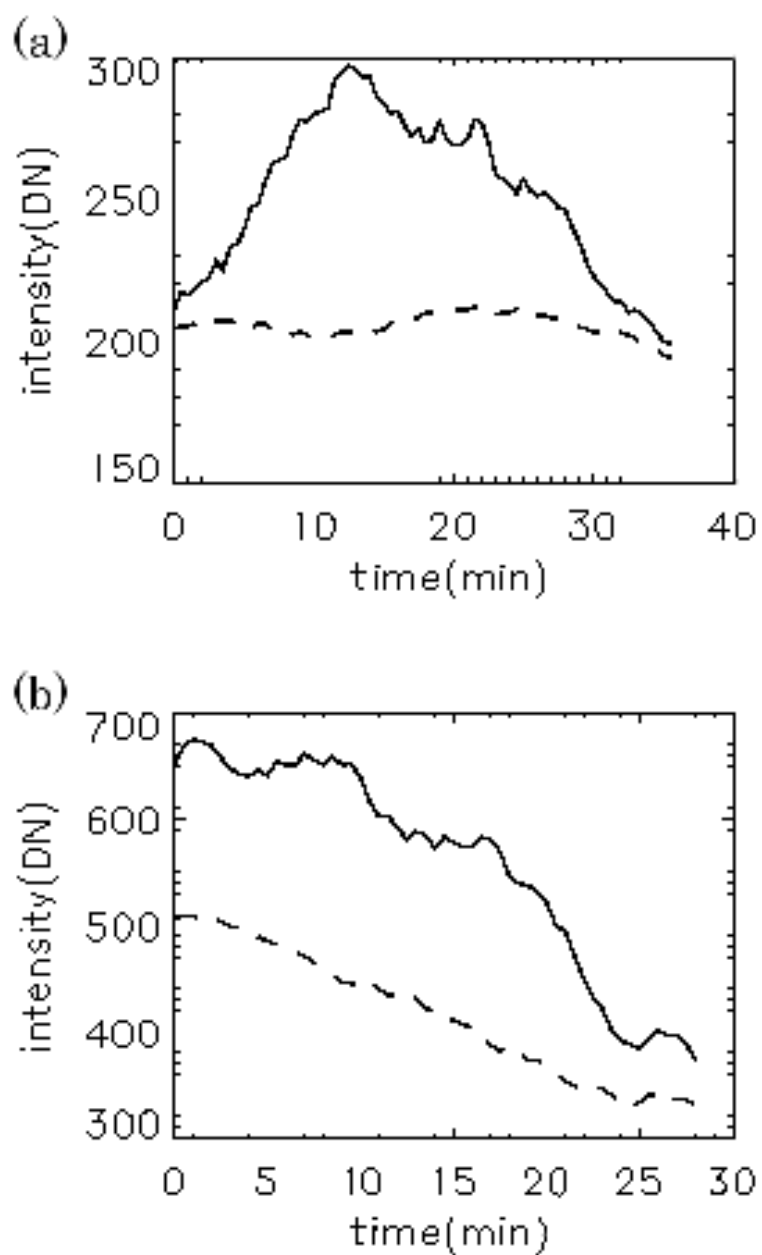


Fig. 2.9.— Light curve of a typical UD. (a) UUD/LUD. (b) PUD. Dashed line indicates the local background brightness.

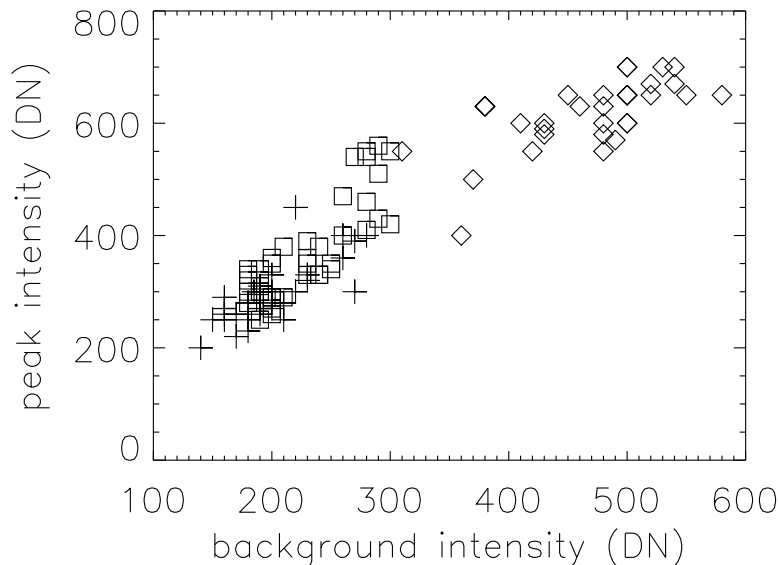


Fig. 2.10.— Scatter diagram of the peak brightness of UDs against their background brightness. Plus-, square- and diamond-symbols denote UUD, LUD and PUD, respectively.

As UDs might be smaller than $0.24''$ (Sobotka et al. 1997a; Sobotka & Hanslmeier 2005), fusion and fission events may be due to temporal brightness variation inside an unresolved cluster of much smaller UDs. Fusion/fission may correspond to brightening/decaying phase of such a cluster of UDs.

2.5. Discussion

From their simulation of three-dimensional non-linear magnetoconvection in a strongly stratified compressible layer, Weiss et al. (2002) made two important suggestions on the internal structure of sunspots. The first one was that UDs are manifestations of small scale convective cells, whose sizes are reduced strongly compared to normal granules by the strong magnetic field. The second one was that diffuse background components, which are larger in size than UDs, correspond to clumps of vigorously convecting plumes, from which magnetic flux is expelled. According to their suggestion, the umbral area is separated into (a) regions of strong fields and small-scale convection and (b) regions of weak fields and large-scale vigorous convection. Spectroscopic observations of the magnetohydrodynamic (MHD) nature of UDs have been done by several researchers. Wiehr & Degenhardt (1993) and Socas-Navarro et al. (2004) concluded that the magnetic field strength is weaker and that small or virtually no upflows exist in UDs, while Lites et al. (1991) detected no indication of a reduced field

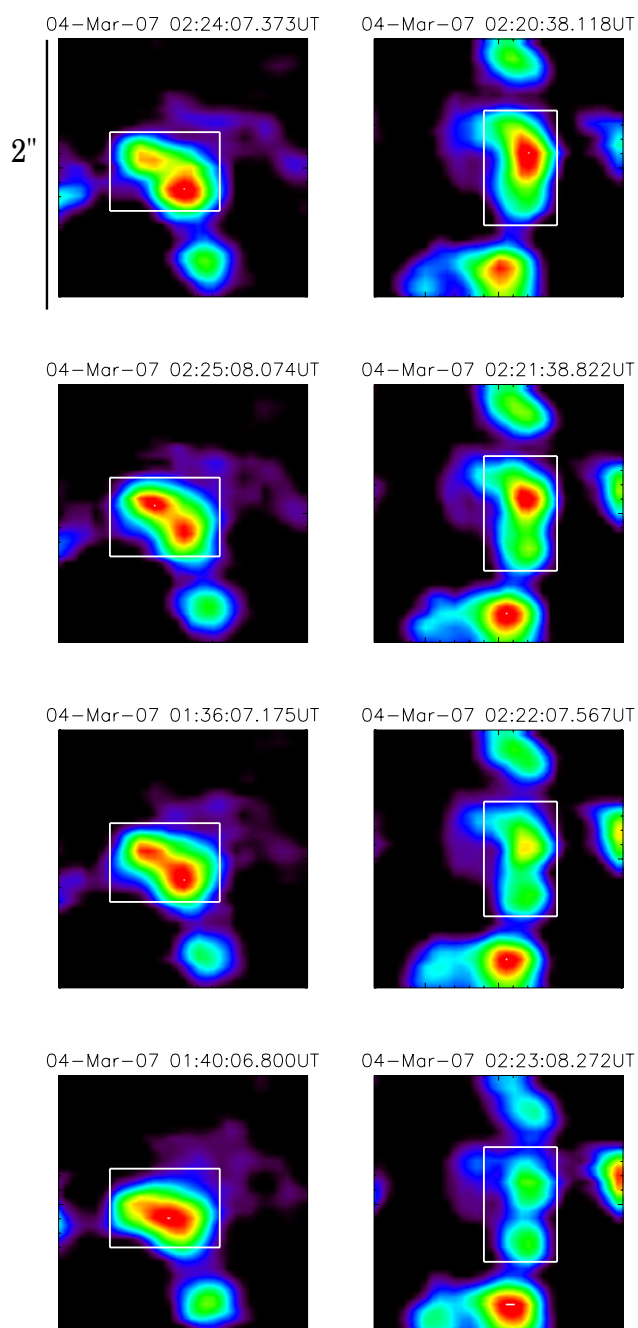


Fig. 2.11.— Temporal evolution of fission and fusion of UD's shown in pseudo-color. Left column shows the fusion of two UD's, while right column shows the fission of another UD. From all the images, background intensities were subtracted to enhance the dot structure.

strength in UDs. It seems that no comprehensive observational view of MHD behavior of UDs is available at present. Especially the differences of the MHD behavior among the types of UUD/LUD/PUD are unknown.

As was suggested in previous work and confirmed in our present observation, PUDs have a different characteristics from UUDs/LUDs regarding their origin, and proper motion. As UUDs/LUDs are immobile and hotter than their surroundings, they probably correspond to small-scale magnetoconvection in a strong magnetic field, as was suggested by Weiss et al. (2002). On the other hand, PUDs show systematic proper motions from the penumbrae to the umbrae and seem to be a natural extension of the so called penumbral grains. We think that the interchange instability model for penumbrae by Schlichenmaier et al. (1998) explains PUDs well. However, one important point remains unclear; UUDs/LUDs and PUDs have a common size of around 200-400km. Why do UUDs/LUDs of magnetoconvective origin in umbrae and PUDs of penumbral origin have nearly the same geometrical sizes? What are the physical processes which determine the UD size of 200-400km? Is there a common mechanism which controls the sizes of the fine structures both in umbrae and penumbrae?

Diffuse components are observed to be hotter than the dark core of umbrae. So they probably correspond to plumes of vigorous convection with weak magnetic flux, as was suggested by Weiss et al. (2002). As LUDs, located in these diffuse components, are observed to have much higher temperatures than UUDs, we suspect that convection is stronger in these diffuse components. However, according to Weiss et al. (2002), small-scale convective plumes, i.e., UDs, are not expected to appear in large-scale vigorous plumes of convection. This expectation contradicts our observations, since we observed many UDs inside the diffuse components. In our three-day observation, diffuse components and dark cores kept their identities. From the analysis of the temporal evolution of many sunspots, Garcia de la Rosa (1987) suggested that sunspots consist of a cluster of several large fragments and that these fragments keep their identities over their whole lifetime. In the fragments, UUDs are formed as was suggested by Weiss et al. (2002). At the interfaces of the fragments, convection from deeper layers is expected to intrude these interfaces, resulting in rather bright diffuse components.

In both the vigorous convective plumes model by Weiss et al. (2002) and the fragment model by Garcia de la Rosa (1987), the occurrence of LUDs in diffuse components remains unexplained. It may be related to the question why UDs have common geometrical sizes irrespective of their types. A mechanism similar to the interchange instabilities proposed by Schlichenmaier et al. (1998) may be at work to form UDs, in addition to magnetoconvection.

Our conclusions and suggestions stated above, including the conjecture of the absence of UDs in the dark core (Lites et al. 1991), need to be studied in further observation and analysis. In next section, we will report on our investigation of the spectropolarimeter data obtained for the same sunspot by *Hinode*/SOT. The temporal evolution of the vector

magnetic field and the Doppler velocities in and around the UDs will allow us more conclusive views of magnetoconvection in sunspots.

REFERENCES

- Garcia de La Rosa, J. I. 1987, *Sol. Phys.*, 112, 49
- Ichimoto, K., et al. 2004, *SPIE*, 5487, 1142
- Kitai, R. 1986, *Sol. Phys.*, 104, 287
- Kosugi, T., et al. 2007, *Sol. Phys.*, 243, 3
- Lites, B. W., Bida, T. A., Johansson, A., Scharmer, G. B. 1991, *ApJ*, 373, 683
- Muller, R. 1979, *Sol. Phys.*, 61, 297
- Schlichenmaier, R., Jahn, K., Schmidt, H. U. 1998, *A&A*, 337, 897
- Sobotka, M., Bonet, J. A., Vazquez, M. 1992a, *A&A*, 257, 757
- Sobotka, M., Bonet, J. A., Vazquez, M. 1992b, *A&A*, 260, 437
- Sobotka, M., Bonet, J. A., Vazquez, M. 1993, *ApJ*, 415, 832
- Sobotka, M., Brandt, P., Simon, G. W. 1997a, *A&A*, 328, 682
- Sobotka, M., Brandt, P., Simon, G. W. 1997b, *A&A*, 328, 689
- Sobotka, M., Hanslmeier, A. 2005, *A&A*, 442, 323
- Socas-Navarro, H., Martinez Pillet, V., Sobotka, M., Vazquez, M. 2004, *ApJ*, 614, 448
- Thomas, J. H., Weiss, N. O. 2004, *ARA&A*, 42, 517
- Weiss, N. O., Proctor, M. R. E., Brownjohn, D. P. 2002, *MNRAS*, 337, 293
- Wiehr, E., Degenhardt, D. 1993, *A&A*, 278, 584
-

3. Magnetic Structure of Umbral Dots²

3.1. Scientific Background

Sunspots are one of the most prominent structures in the solar photosphere. However, there are many unsolved problems related to them even today. A particular one is the source of energy transport in sunspots. It is known that the radiative energy alone is not sufficient to account for the observed brightness of sunspots, so another form of convective energy transport is necessary (Deinzer 1965). The study of umbral dots (UDs), tiny bright points in the umbra, is essential for understanding the energy transport in sunspots, since UD are considered to be a manifestation of convection.

Parker (1979) suggested in his “spaghetti” model that UD are the radiative signatures of the top parts of field-free convective plumes. The field-free plumes emerge from below the visible surface into a gap between magnetic bundles in a cluster-type sunspot. These plumes are accompanied by smaller magnetic field strengths, substantial upflows within the UD, and a cusp-shaped magnetic structure (Spruit & Scharmer 2006). Another promising model is the magneto-convection in monolithic sunspots. The monolithic model considers a sunspot as the aggregation of uniform, vertically thin columns. Accordingly, UD are considered as a natural result of the overstable oscillatory convection, which is the preferred mode just below the photosphere (Weiss et al. 2002; Schüssler & Vögler 2006). The monolithic model predicts smaller field strengths, upflows in the center of UD in addition to downflows at their boundaries, and a cusp-like structure.

Few spectroscopic observations of UD have been carried out so far, because of their limited size (less than 0.5”) and low brightness. Only in recent days, some spectroscopic work has been published (Pahlke & Wiehr 1990; Lites et al. 1991). Wiehr & Degenhardt (1993) observed UD in the lines Fe 6843Å and Ca 6103Å and found a reduction of a field strength up to 20% and a flatter field inclination in the lower layer. Weaker fields (~ 500 Gauss) with more horizontal orientations ($\sim 10^\circ$) in UD were reported in Socas-Navarro et al. (2004).

As for the Doppler velocity field, substantial upward velocities ($\sim 1 \text{ km s}^{-1}$) are observed in the lower photosphere. However, for the lines formed in the upper photosphere, no strong velocity field can be related to individual UD. Rimmele (2004) found upflows in excess of 1 km s^{-1} in C I 5380Å line (lower photosphere), while no strong upflow in Fe I 5576Å line (upper photosphere) could be seen. Socas-Navarro et al. (2004) also found upflows of $\sim 250 \text{ m s}^{-1}$ in Fe 6303.46Å (lower photosphere) line, and no obvious upflows in Fe 6302.5Å line

²This chapter is based on a paper accepted for publication by PASJ, entitled “Magnetic Structure of Umbral Dots Observed with Hinode Solar Optical Telescope”

(upper photosphere). Recently, Bharti et al. (2007a) recorded upward velocities of the order of 400 m s^{-1} , surrounded by narrow downflow regions with $\sim 300 \text{ m s}^{-1}$ in Fe I 5576Å line.

The spectro-polarimeter (SP) on-board *Hinode* SOT (Tsuneta et al. 2008; Suematsu et al. 2008; Ichimoto et al. 2008; Shimizu et al. 2008) made it possible to observe diffuse UDs at the center of the umbra, with a resolution limit of $0.3''$ in a highly stable condition. We derived magnetic field strengths, orientations of the magnetic field, filling factor, and Doppler velocities using the Milne-Eddington inversion code (Yokoyama et al. 2008, in preparation). In the following sections, we describe the details of the observation (§3.2), analyze the Stokes V area asymmetry (§3.3), and show the statistical results for the magnetic fields and the Doppler fields of UDs (§3.4). Finally, in §3.5, we discuss and summarize our findings in the framework of two theoretical models, the monolithic model (Schüssler & Vögler 2006) and the field-free intrusion model (Spruit & Scharmer 2006).

3.2. Observation

The SP observation was carried out from March 2 through March 4, 2007, in parallel with the acquisition of the filtergram data, analyzed in Kitai et al. (2007). The target was NOAA 10944 with an α -type sunspot in its decaying phase. The sunspot invoked neither flaring nor surging activity, and almost disintegrated on March 5. The region was located on the west side of the solar surface. The heliocentric coordinate of NOAA 10944 was ($S6^\circ$, $W17^\circ$) on March 2, ($S5^\circ$, $W30^\circ$) on March 3, and ($S6^\circ$, $W43^\circ$) on March 4, respectively.

With the SP, a Normal Map mode observation was carried out from 00:10 UT to 00:50 UT on the three consecutive days. The Normal Map mode scans an area with an integration time of 4.8s per slit position. The observation covers a field-of-view (FOV) of $80'' \times 80''$ with a polarimetric accuracy of 0.1%. The spatial pixel size was $0.159''$ in slit direction and $0.147''$ in step direction. The spectral FOV covers two absorption lines, Fe I 6301.5Å ($g_{\text{eff}} = 1.66$) and Fe I 6302.5Å ($g = 2.5$). The SSW routine *sp_prep.pro* was applied for the purpose of dark field subtraction and flat fielding.

3.3. Stokes V area asymmetry

Figure 3.1 (*top*) shows the map of the Stokes V area asymmetry in Fe I 6302.5Å line on March 2. The area asymmetry of the Stokes V profiles indicates either the large gradient of the field strength or the line-of-sight velocity (Solanki & Stenflo 1984, Stenflo & Harvey 1985; Grossmann-Doerth et al. 1988, 1989; Sánchez Almeida & Lites 1992). We adopted the definition of the Stokes V area asymmetry (δA) as

$$\delta A = \frac{\int_{blue} |V| d\lambda - \int_{red} |V| d\lambda}{\int_{blue} |V| d\lambda + \int_{red} |V| d\lambda} \quad (3.1)$$

where each integration is performed over the area of the blue or red lobe of the V profiles. In the dark core region ($x=250''$, $y=0''$), δA is noisy, probably due to the blending of molecular lines at low temperatures. Except for the dark core, the umbra has a negligible value of δA . This is because of the suppression of convective motions in the presence of strong magnetic fields, which produces a small line-of-sight velocity in the umbra. Morinaga et al. (2007) reported a smaller asymmetry in the center of pores than in its surrounding, which is consistent with our result.

3.4. Magnetic Structure and Doppler Velocity Distribution around UDs

3.4.1. Inversion

We applied a Milne-Eddington inversion code (Yokoyama et al. 2008, in preparation) to the Stokes spectra. As the Stokes V profile in the umbra has a negligible area asymmetry (§3.3), it is reasonable to assume a Milne-Eddington atmosphere. The best-fit UD profiles at the position (a) indicated in Fig. 3.1 (*bottom*) are shown in Fig. 3.2. The figure shows that the Milne-Eddington inversion produces excellent fits to the observations. The inversion code can derive 10 free parameters: three components of the magnetic field (strength, inclination, and azimuth angle), line-of-sight velocity, two parameters describing the linear dependence of the source function on the optical depth, line strength, Doppler width, damping parameter, macroturbulent velocity, stray-light fraction, and a shift of the stray-light profile. The 180° ambiguity of the azimuth angle is determined by a comparison with the potential fields calculated from the line-of-sight component of the magnetic field. The stray-light profile is given by a Stokes I profile averaged over the regions where the maximum polarization degree ($p = \sqrt{Q^2 + U^2 + V^2}$) along the line profile is larger than 0.2%. The stray-light represents the effect of a degradation of the polarization signal due to telescope diffraction and insufficient angular resolution (Orozco Suarez et al. 2007). The magnetic filling factor, which represents the fraction of magnetized atmosphere, is computed as $1 - (\text{stray-light fraction})$. The 2D maps and magnetic field vectors are converted to local coordinates referring to the solar surface with the assumption that the solar surface is flat in our field of view. In the following, maps are presented as seen from the top. The Doppler velocity is subtracted from the average Doppler velocity value inside the umbra. The observed Doppler velocity field includes 3min umbral oscillation, 5min p-mode oscillation, and other instrumental effects. We did not remove these effects, since our interest lies in the local variations around UDs from them, which can be easily distinguished (umbral oscillation, p-mode, etc.).

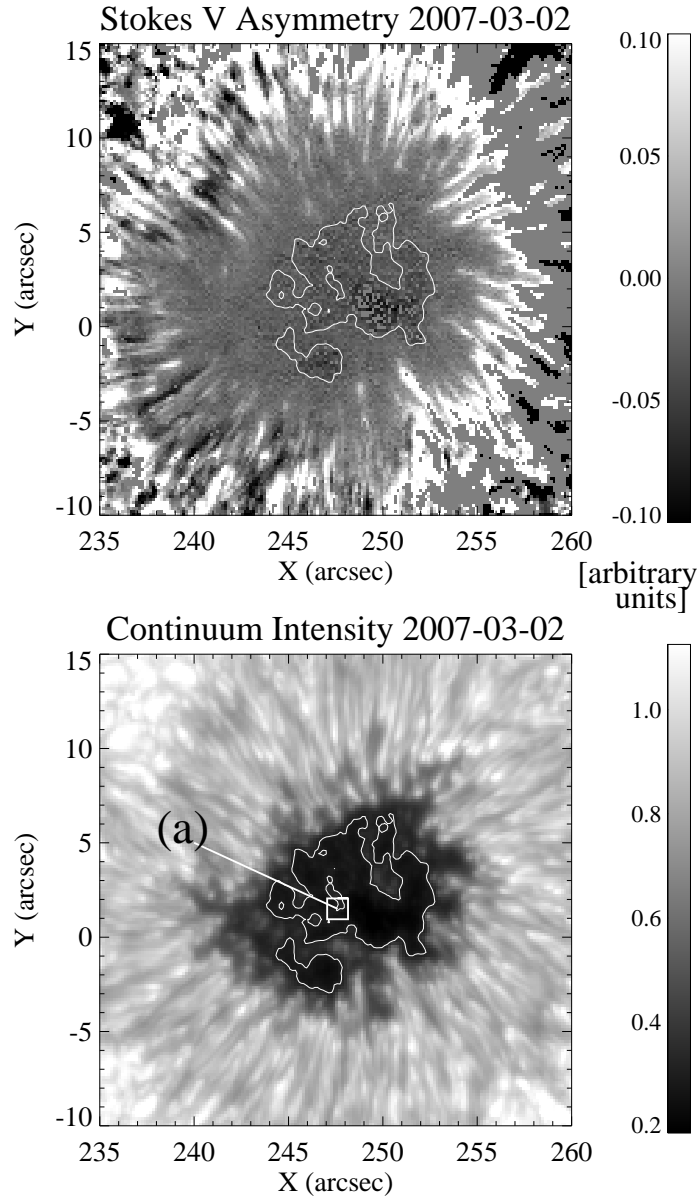


Fig. 3.1.— Stokes V area asymmetry map (*top*) and continuum map at 6303\AA (*bottom*) on March 2. The white curves show the smoothed contours of the continuum intensity at a level of 30% of I_{quiet} . Here, I_{quiet} is the average intensity of the quiet region. The brightness of the continuum map is normalized by I_{quiet} . The Stokes profiles at the position (a) are shown in Fig. 3.2.

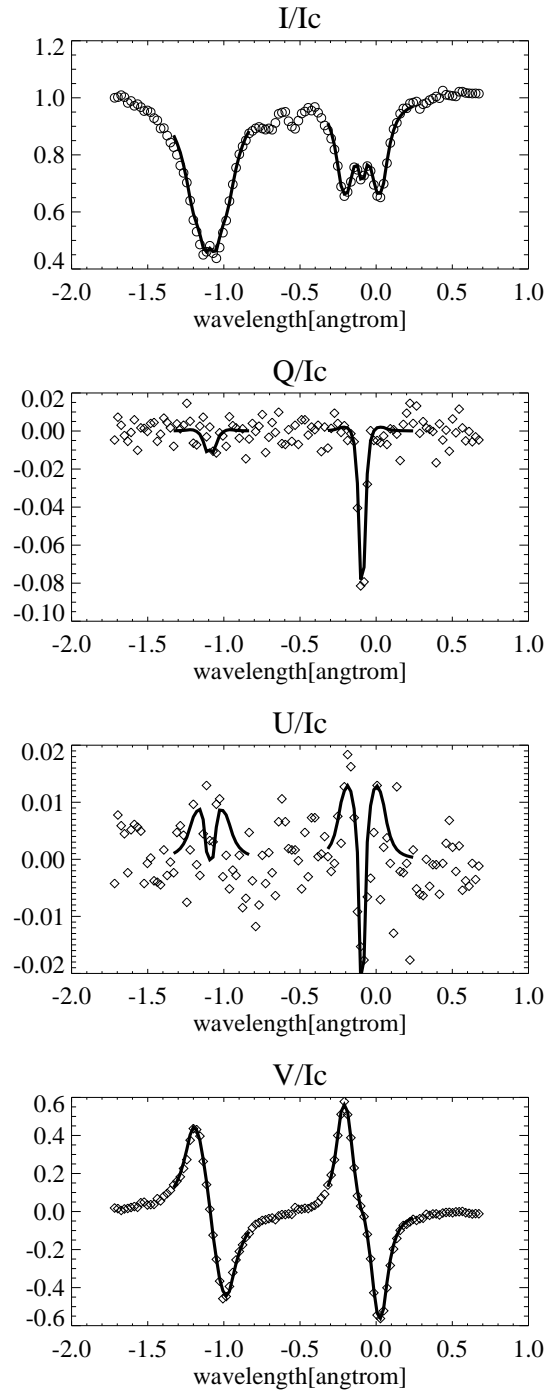


Fig. 3.2.— Observed (*diamonds*) and best-fit Stokes I , Q , U , V profiles (*solid lines*) by inversion at the position (*a*), as indicated in Fig. 3.1. The profiles are normalized by the Stokes I intensity at continuum wavelength $\lambda \sim 6303\text{\AA}$ (I_c).

We estimated the random error levels of the derived physical quantities from the standard deviation of the original map after subtracting a boxcar smoothed map (width is $0.3'' \times 0.3''$) inside the umbra. The smoothing width ($0.3'' \times 0.3''$) is chosen to be narrower than the typical UD size in order to calculate the fluctuation level contribution from other sources. As a result, the 1σ error levels of the field strength, the field inclination, the Doppler velocity, and the filling factor are 13 Gauss, 0.7° , 10 m s^{-1} , and 0.02, respectively.

3.4.2. Identification of UDs

To identify UDs, we adopted the image segmentation method explained in Sobotka et al. (1997). First, we constructed a boxcar smoothed continuum map (4×4 pixels). Then, the original continuum map was divided by the smoothed one, that is, $I_c(\text{original})/I_c(\text{smoothed})$. I_c is the Stokes I intensity at continuum wavelength. We employ an empirical threshold value of 1.05 for identifying UDs, that is, an UD is more than 1.05 times brighter than its vicinity. To suppress the statistical noise, UDs whose areas are less than 3 pixels are excluded from the analysis. In doing so, we identified 27 UDs on March 2 (Fig. 3.3), 35 on March 3, and 25 on March 4. In total, 87 UDs are analyzed in this paper.

In Kitai et al. (2007), UDs are classified into 3 categories by their creation site, i.e., umbra, penumbra, and light-bridge. The three categories of UDs show different characteristics with respect to their proper motion and temperature. However, we don't take care of the subclasses in this paper, since we can not trace the birth site of each UD with our data sets.

3.4.3. Statistics over three days

We derived spatial profiles of the continuum intensity, the field strength (B), the field inclination (i), the filling factor (f), and the Doppler velocity (v) across each UD in the direction of the horizontal component of the magnetic field (shown in Fig. 3.3 with arrows). The plots for the UD (b), marked in Fig. 3.3, are shown in Fig. 3.4. The horizontal axis covers the spatial length of $2.2''$ (15 pixels), which is large enough to cover the entire UD. First, we determined the position of the UD (x_{UD}) and its background (x_{BG} , 2 points at both side) by eye inspection of the local maximum and local minima of the continuum intensity (Fig. 3.4, *top*). Second, we calculated $\Delta F = F(x_{UD}) - F(x_{BG})$, where $F = B, i, f, \text{ or } v$.

Figure 3.5 displays the histograms of the difference values (ΔF) of the four physical parameters. In the statistical average of the three day's data, UDs show relative blue shifts ($\Delta v_{\text{average}} = -18 \text{ m s}^{-1}$). For the magnetic field, however, the statistical averages ($\Delta B_{\text{average}} = -7 \text{ Gauss}$, $\Delta i_{\text{average}} = 0.2^\circ$, $\Delta f_{\text{average}} = 0.007$) are smaller than the error levels, i.e., 13 Gauss, 0.7° , and 0.02, respectively.

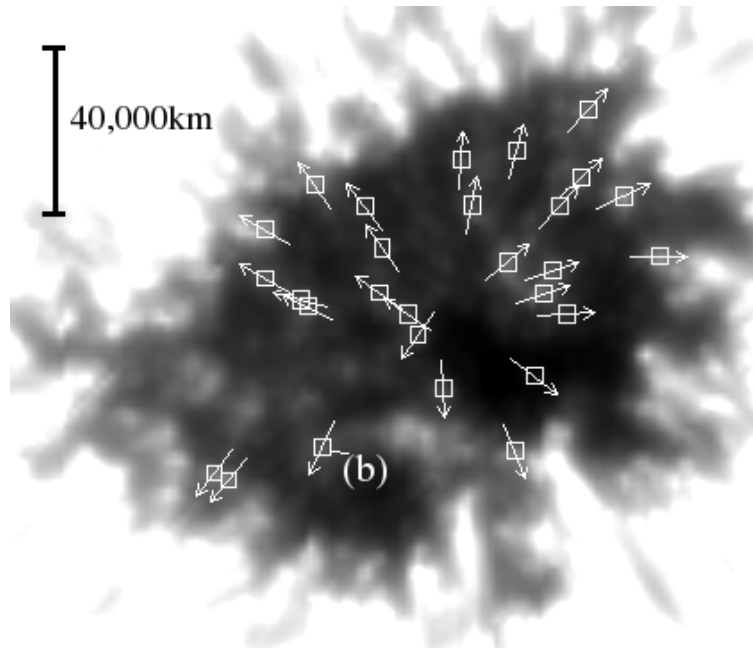


Fig. 3.3.— Positions of 27 identified UD's on March 2. The directions of the arrows correspond to the horizontal orientation of the magnetic field at each position. The UD at position (*b*) is investigated further in Fig. 3.4.

In Fig. 3.6, we show four scatter plots (from top to bottom: field strength ΔB , field inclination Δi , filling factor Δf , and Doppler velocity Δv) against the continuum intensity ratio UD/BG. A larger continuum intensity ratio means a brighter UD. Red (March 2), green (March 3), and blue (March 4) circles indicate the average values in intensity ratio bin $\Delta(\text{UD/BG})=0.2$ with error bars showing the standard deviation. Apparently, no correlation exists between the continuum intensity ratio and Δi or Δf (second and third panels of Fig. 3.6). On the other hand, ΔB and Δv are weakly correlated to the continuum intensity ratio (top and bottom panels of Fig. 3.6). That is, brighter UD's have weaker magnetic fields and larger blue shifts.

3.4.4. Center-to-limb variation

As stated in §3.4.3, the UD's magnetic field, compared to their surroundings, does not show distinct variations in the statistical average of the three days's data. However, we found an interesting property in the daily statistics. The difference values ΔF show center-to-limb variation, as listed in Table 3.1. $|\Delta B|$, $|\Delta i|$, and $|\Delta v|$ decreases from day to day, but Δf does not. The sunspot was the closest to disk center on March 2. Observed near disk center,

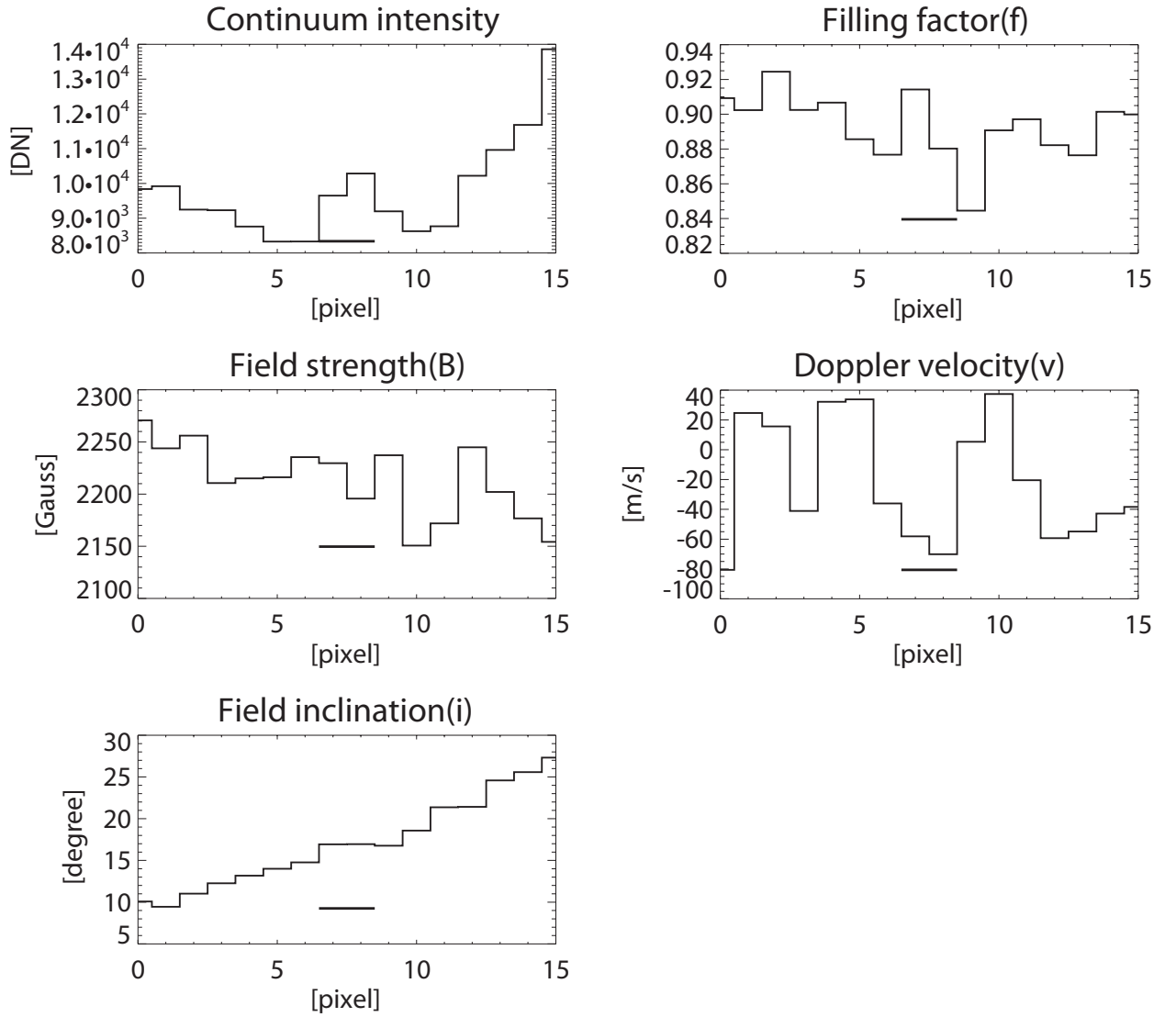


Fig. 3.4.— Five plots around the UD indicated as (b) in figure 3.3. For the Doppler velocity plot, positive values mean downflows. A thick bar below each plots indicates the span of pixels which satisfy UD's conditions stated in §3.4.2. $x_{UD} = 8, x_{BG} = [5, 10]$. $B_{UD} = 2196 \text{ Gauss}$, $B_{BG} = 2183 \text{ Gauss}$, $i_{UD} = 17.0^\circ$, $i_{BG} = 16.3^\circ$, $f_{UD} = 0.880$, $f_{BG} = 0.888$, $v_{UD} = -70.1 \text{ m s}^{-1}$, $v_{BG} = 35.6 \text{ m s}^{-1}$.

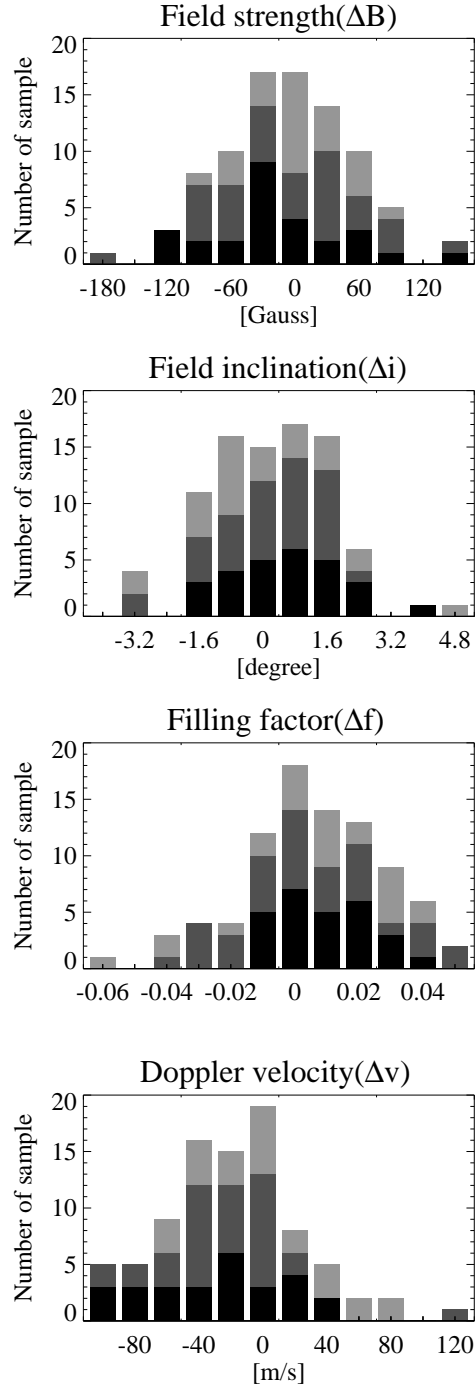


Fig. 3.5.— Histograms of UD–BG differences. The total sample number is 87. From top to bottom: field strength (ΔB), field inclination (Δi), filling factor (Δf), and Doppler velocity (Δv). The black, gray, and light gray bars indicate the UDs on March 2, 3, and 4, respectively.

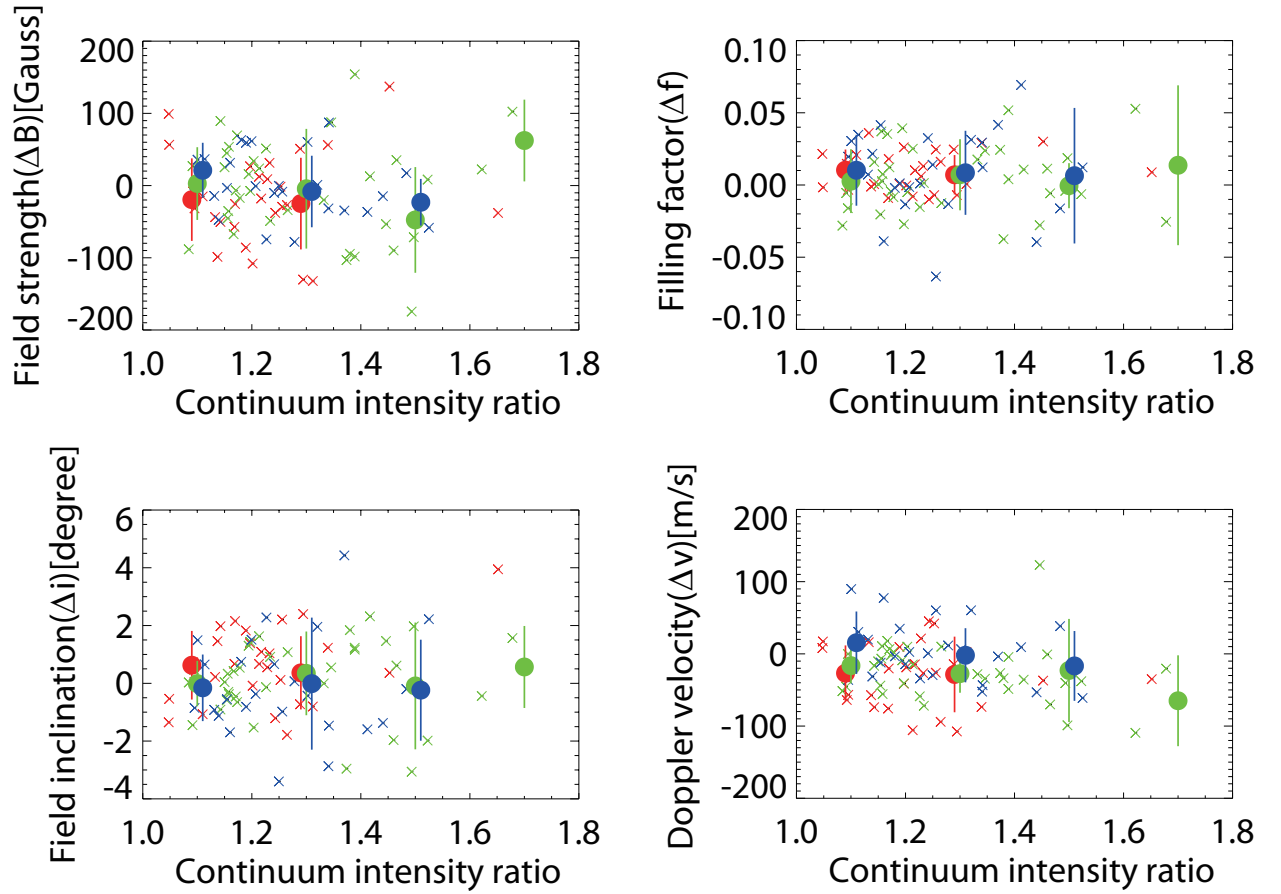


Fig. 3.6.— Scatter plots of field strength (ΔB), field inclination (Δi), filling factor (Δf), and Doppler velocity (Δv) against continuum intensity ratio UD/BG. Crosses indicate UDs on March 2 (red), March 3 (green), and March 4 (blue). Circles show the average values in the intensity ratio bin $\Delta(\text{UD/BG})=0.2$ in each of the three observing days. The colored, solid lines show the standard deviation error bars. A negative value of Δv means blue shift.

UDs show smaller field strength, larger field inclinations (i.e., more horizontal), and showed relative blue shifts. On March 4, the sunspot was more distant from the disk center. In this case, UDs and their BG show almost no difference in their magnetic fields and Doppler fields. In the case of the Doppler velocity, however, this result might be caused partially by a projection effect, since we measure the line-of-sight velocities.

3.5. Discussion and Summary

Our analysis revealed the magnetic structure and the velocity field distribution around UDs from seeing-free, high-sensitive *Hinode* SP observation. The main results are as follows:

1. The Stokes V profiles of UDs are virtually symmetric.
2. In the three-day statistical average, UDs do not produce distinct variations in their magnetic conditions compared to their surroundings, while the Doppler velocity shows effective blue shifts (-18 m s^{-1}).
3. The filling factor shows no difference for different UDs.
4. Bright UDs are weakly correlated to weaker field strength and stronger relative blue shift .
5. The local differences in the field strength, the field inclination, and the Doppler velocity of UDs show center-to-limb variation.

3.5.1. Fe I formation height

According to Tritschler & Schmidt (1997), the formation height of the Fe I 6302.5Å line in the umbrae is 180 km higher than the height of continuum optical depth $\tau_C = 1$ at 500nm for the line core, while this value reduces to 130 km in case of the UD. In addition, the continuum emission layer of the UD is located ~ 100 km higher than that of the umbra (Degenhardt & Lites 1993). However, these values are estimated at disk center, where we can look into the deepest layer. Closer to the limb, the formation height of the spectral lines gets higher and higher. This may explain the center-to-limb variation in UDs we found in §4.3.2. The schematic view of an UD that accounts for the center-to-limb variation of magnetic fields and velocity fields is shown in Fig. 3.7. When we observe an UD at the disk center, weakly-magnetized hot gas can reach the formation height of Fe I. The observation reveals smaller field strengths ($\Delta B = -17 \text{ Gauss}$), flatter field inclinations ($\Delta i = 0.6^\circ$), and stronger relative blue shifts ($\Delta v = -28 \text{ m s}^{-1}$), though the field inclination differences are less than the error fluctuation level. When we observe an UD far from the disk center, the

Table 3.1: Center-to-limb variation of the averaged difference value UD–BG

	March 2 S6°,W17°	March 3 S5°,W30°	March 4 S6°,W43°
Field strength ΔB [Gauss]	–17	–6	1
Field inclination Δi [degree]	0.6	0.1	–0.1
Filling factor Δf	0.009	0.004	0.009
Doppler velocity Δv [m s ^{–1}]	–28	–24	3

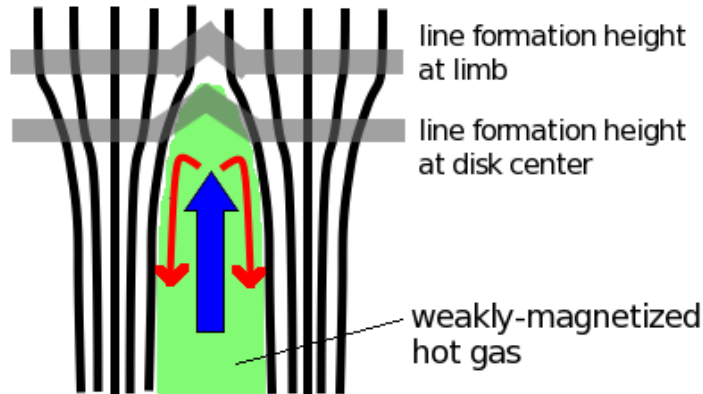


Fig. 3.7.— Schematic figure of the cusp-shaped UD magnetic field lines and the Fe I line formation height. The black solid lines are magnetic field lines. The central green part corresponds to a weakly-magnetized hot gas, i.e., an UD. Blue and red arrows indicate upflows and downflows, respectively. The downflows, however, could not be confirmed with our study. The two gray thick lines indicate the line formation heights at the disk center (lower) and at the limb (upper). See text for further information.

line formation height is higher than the UD occurring site. Our observations support this interpretation, because we could not find large differences between UDs and their BG on March 4. Our results follow the model in which UDs are formed deep in the photosphere and have a cusp-shaped magnetic field. The downflows, denoted with red arrows in Fig. 3.7, are discussed in §3.5.3.

There exist the possibility that this center-to-limb variation is due to the evolutionary phase difference of UDs in a decaying sunspot. Thus far, to the best of our knowledge, no one has examined the change of UD characteristics in developing, mature, and decaying sunspots. Of course, the actual cause of this variation might as well be a mixture of the two, that is, the formation height difference and the evolutionary phase difference.

3.6. Filling factor

As stated in §3.4.1, the filling factor is computed as $1 - (\text{stray-light fraction})$. In our inversion model, the stray-light profile is given by a Stokes I profile averaged over the regions where the maximum polarization degree along the line profile is larger than 0.2%. According to the limb observation of SP performed on March 16, 2007, the fraction of the scattered light in the continuum wavelength was 2% at a location a few arcsec away from the limb. On the other hand, the average stray-light fraction inside the umbra was $\sim 10\%$. Thus, the observed profile is considered to be composed of three components: unpolarized light due to telescope diffraction ($\sim 2\%$), unpolarized light from the field-free atmosphere in the umbra, and polarized light from the magnetized gas. The filling factor indicates the fraction of the polarized light.

Assuming that UDs are a penetration of field-free hot gas (Socas-Navarro et al. 2004; Spruit & Scharmer 2006) and that the penetration reaches the formation height of Fe I 6302Å, the detection of small filling factors for UDs are predicted. However, we could not find such a decrease of the filling factor for UDs (Table 1 and Fig. 3.6). Higher resolution observations are strongly required for further discussion.

3.7. Comparison with sunspot models

3.7.1. The monolithic model

A three dimensional simulation of UD phenomena was recently carried out by Schüssler & Vögler (2006). They explained UDs as a natural result of convection in a strong, initially monolithic magnetic field. In their simulation, most of the UDs had an elongated form with a central or threefold dark lane, which separates the UD into two or three parts. At the end points of the dark lane there exist downflow patches.

This picture is rather different from our observational results: We observed almost circular UDs, showing no dark lanes, in the Fe I continuum map. This is also the case for the blue/green continuum images obtained with *Hinode* SOT with a spatial resolution $0.2''$ (Kitai et al. 2007). However, in recent days, some evidence of dark lanes has been found from high resolution data (for example, Bharti et al. (2007b) with G-band filtergrams using *Hinode* SOT). Thus far, no one succeeded in finding localized downflow patches at the end points of dark lanes (see Fig. 1 in Schüssler & Vögler 2006). There are two possibilities for this disagreement: one is that the downflow patches may be too small to be detected with *Hinode*'s resolution limit. The other one is that the signal of the Stokes profile becomes too faint to be detected because the continuum intensity (i.e., temperature) decreases when the gas flows downward.

We found another important phenomenon of UDs. It is already known empirically that some UDs occur and recur at the same location (Rimmele 1997). With *Hinode*'s seeing-free conditions we observed the light curve of successive UDs for about 3 hours using green continuum data. Some UDs, located in the center part of the umbra, showed oscillatory light curves. One example is shown in Fig. 3.8. The characteristic period of the oscillation is ~ 10 minutes, and the successive emergence of UDs continues over ~ 50 minutes. These intensity oscillations support the monolithic model, because this model predicts from a linear stability analysis (Weiss et al. 1990) that oscillatory convection is the preferred mode in the first few Mm depth below the umbral photosphere.

3.7.2. The field-free intrusion model

Another plausible scenario for UDs is the field-free intrusion model. This model was proposed in Parker (1979), where he discussed that the magnetic field lines beneath the umbra are divided into many separate flux tube bundles, like “spaghetti”. In this picture, the UDs are a manifestation of field-free hot gas intrusion from deeper layers through gaps in the nonuniform magnetic field.

A numerical study of the field-free intrusion model was carried out by Spruit & Scharmer (2006) for penumbral grains and an observational study was performed by Rimmele (2008). Spruit & Scharmer (2006) predict cusp-shaped magnetic field lines, weaker magnetic field, and upflows within the cusp. These characteristics of UDs are almost the same as those of the monolithic model, apart from the localized downflow patches: the field-free intrusion model also predicts downflows based on radiative cooling, but not concentrated on localized patches. The weak correlation between dark UDs and downward motions, shown in Fig. 3.6, may be evidence for downflow by radiative cooling. As for the oscillatory light curve (Fig. 3.8), however, the field-free intrusion model fails to predict such oscillations. It would be highly advantageous if future numerical simulations can clarify the possibility of brightness oscillations in the field-free hot gas, surrounded by strong umbral magnetic fields.

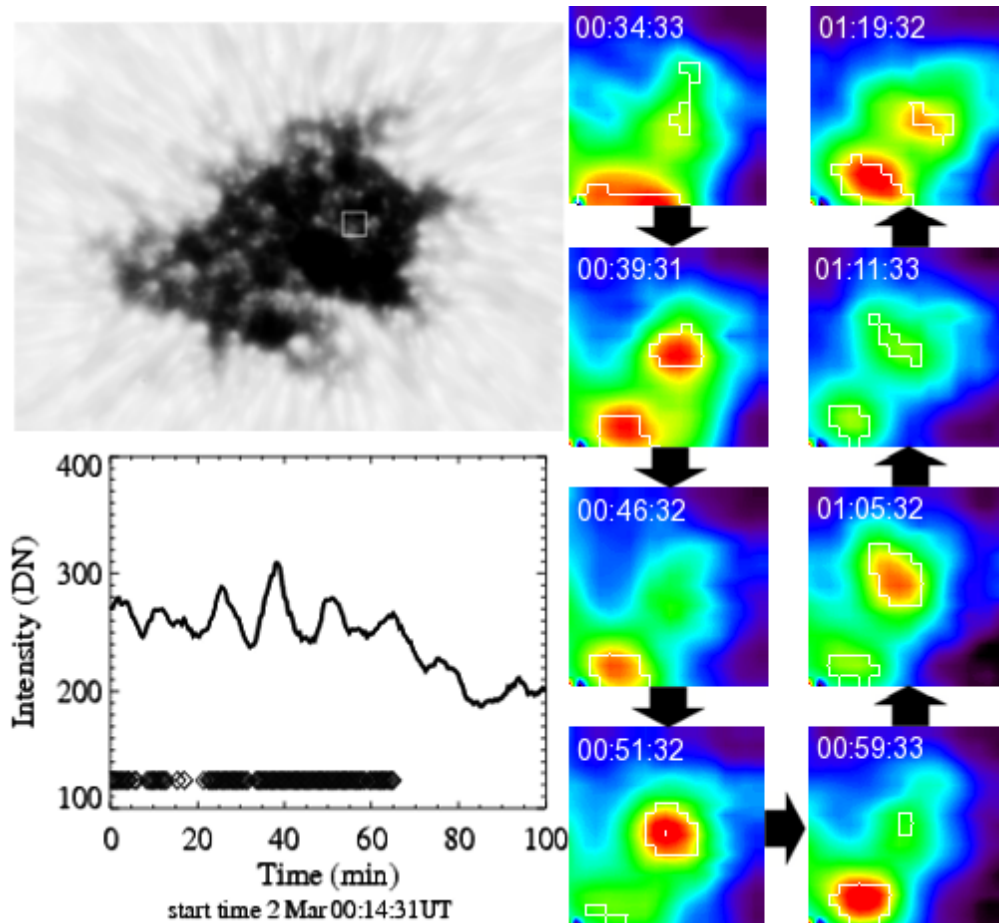


Fig. 3.8.— Upper left: green continuum image on March 2, 2007. The position of a periodic UD is marked with a white square. Lower left: light curve of the center of the white square. Below the light curve, diamond signs are shown which indicate a brightness of more than 8% than that of the surroundings. Right: Temporal changes the white square region (pseudocolor display). The time is displayed at upper left of each image in UT.

As we discussed in this paper, the oscillatory brightening of UDs seems to be a key phenomenon to reach a firm conclusion on the origin of UDs. Detailed numerical studies and higher resolution observations, including a spectroscopic study of the temporal evolution of these phenomena, are strongly required in the near future.

In this study, we detected many meaningful observational properties of magnetic field around UDs. This success of our investigation, in particular in deriving good correlations between UDs and the components of the magnetic field, owes greatly to the stable, sensitive, and high-resolution observation performed with the spectro-polarimetry on-board the *Hinode* Solar Optical Telescope.

REFERENCES

- Bharti, L., Jain, R., & Jaaffrey, S. N. A. 2007a, ApJ, 665, L79
- Bharti, L., Jain, R., & Jaaffrey, S. N. A. 2007b, ApJ, 669, L57
- Degenhardt, D., & Lites, B. W. 1993, ApJ, 404, 383
- Deinzer, W. 1965, ApJ, 141, 548
- Grossmann-Doerth, U., Schüssler, M., & Solanki, S. K. 1988, A&A, 206, L37
- Grossmann-Doerth, U., Schüssler, M., & Solanki, S. K. 1989, A&A, 221, 338
- Ichimoto, K., et al. 2008, Sol. Phys., 249, 233
- Kitai, R., et al. 2007, PASJ, 59, S585
- Lites, B. W., Bida, T. A., Johanesson, A., & Scharmer, G. B. 1991, ApJ, 373, 683
- Morinaga, S., et al. 2007, PASJ, 59, S613
- Orozco Suarez, D. ., et al. 2007, PASJ, 59, S837
- Pahlke, K. D., & Wiehr, E. 1990, A&A, 228, 246
- Parker, E. N. 1979, ApJ, 234, 333
- Rimmele, T. 1997, ApJ, 490, 458
- Rimmele, T. 2004, ApJ, 604, 906
- Rimmele, T. 2008, ApJ, 672, 684

- Sánchez Almeida, J., & Lites, B. W. 1992, *ApJ*, 398, 295
- Schüssler, M., & Vögler, A. 2006, *ApJ*, 641L, 73S
- Shimizu, T., et al. 2008, *Sol. Phys.*, 249, 221
- Sobotka, M., Brandt, P., & Simon, G. W. 1997, *A&A*, 328, 682
- Socas-Navarro, H., Martinez Pillet, V., Sobotka, M., & Vazquez, M. 2004, *ApJ*, 614, 448
- Solanki, S. K., & Stenflo, J. O. 1984, *A&A*, 140, 185
- Spruit, H. C., & Scharmer, G. B. 2006, *A&A*, 447, 343
- Stenflo, J. O., & Harvey, J. W. 1985, *A&A*, 95, 99
- Suematsu, Y., et al. 2008, *Sol. Phys.*, 249, 197
- Tritschler, A., & Schmidt, W. 1997, *A&A*, 321, 643
- Tsuneta, S., et al. 2008, *Sol. Phys.*, 249, 167
- Weiss, N. O., Brownjohn, D. P., Hurlburt, N. E., & Proctor, M. R. E. 1990, *MNRAS*, 245, 434
- Weiss, N. O., Proctor, M. R. E., & Brownjohn, D. P. 2002, *MNRAS*, 337, 293
- Wiehr, E., & Degenhardt, D. 1993, *A&A*, 278, 584
-

4. Dependence of Umbral Dots on their Magnetic Nature

4.1. Scientific Background

The solar surface is showing ample signatures of convection, for example, solar granules. The solar granules are known to have abnormal shapes in the presence of magnetic fields (Sobotka et al. 1994). Inside sunspots (a few thousand Gauss), normal granules are seen rarely. Umbral dots (UDs) are the counterpart of the granules in the sense that UD is also a signature of magnetoconvection. The term magnetoconvection refers to convection, modified by the presence of a magnetic field. Two-dimensional magnetoconvection in a Boussinesq fluid was studied in detail by Proctor & Weiss (1982), and the systematic investigation of compressible magnetoconvection was described by Weiss et al. (1990). Weiss et al. (1990) revealed that the modes of magnetoconvection are governed by the ratio ζ of the magnetic to the thermal diffusivity. For $\zeta \lesssim 1$, we obtain oscillatory convection with periodic reversals of the flow velocity. For $\zeta \gtrsim 1$, overturning convection occurs with a spatially asymmetric rising and falling of the plumes. In the photosphere, the thermal diffusivity usually exceeds the magnetic diffusivity and ζ is far smaller than unity throughout the convection layer. In the umbra, however, the atmosphere conditions are such that $\zeta < 1$ at the top and $\zeta > 1$ at the bottom. Because of this complex physical state, magnetoconvection in sunspots has been investigated mainly using the computer simulations (Shüssler & Vögler 2006; Heinemann et al. 2007; Rempel et al. 2008).

Now that we carried out the nearly simultaneous observations of the umbra by the filtergram and the spectrogram onboard the *Hinode* satellite, we can study the characteristic dependence of UD on the magnetic field. Our results can serve as useful feedback to a more realistic MHD simulation, probably leading to an ultimate understanding of the subsurface structure of sunspots.

In the following sections, we describe the observations and the data reduction of the *Hinode* SOT blue continuum data (§4.2), explain the UD detection algorithm (§4.3), compare our results to the *Hinode* SOT spectro-polarimeter data (§4.4), and finally give a discussion in §4.5.

4.2. Observation and Data Reduction

The target of our observations was NOAA 10944, which appeared from the east limb on Feb 23, 2007, and disintegrated on Mar 5. We analyzed the time-sequence data of 136 minutes, from 00:14UT till 02:30UT on Mar 1. At that time, the sunspot was located almost at disk center: the heliocentric coordinate of the sunspot at 00:14UT on 1 Mar was ($63''$, $17''$).

We used the blue continuum (4504Å) images taken with the *Hinode* Solar Optical Telescope (Tsuneta et al. 2008). The images were taken with a constant 6s interval. However, since we analyzed every 4th image, the temporal cadence is ~ 25 s in our case. The spatial pixel resolution was $0.054''$. The time of the exposure was relatively long, 102 ms, in order to obtain an appropriate observation of the umbra. The field-of-view (FOV) of the filtergram images was $54'' \times 27''$, which contains the entire umbra.

The time-sequence data consist of 321 images. After the dark field subtraction and the flat fielding, the images were carefully co-aligned by finding the displacements which give the maximum cross-correlation between consecutive frames. The final precision of our co-alignment is sub-pixel. Then, to each image a Hanning filter was applied, cf. the Hanning window: $w(k_x, k_y) = (0.5 - 0.5\cos(2\pi k_x/N_x)) * (0.5 - 0.5\cos(2\pi k_y/N_y))$ ($k_{x,y}$: wave number, $N_{x,y}$: the size of the image, $x, y = 0, 1, 2, \dots, N_{x,y} - 1$) to reduce the high-frequency noise in space caused by CCD or photon noise. Finally, we normalized the images by the low-frequency component of the averaged lightcurve of the quiet-sun region. In doing so, we removed the effect of the orbital variation of the *Hinode* whose period is ~ 96 minutes.

In addition to the filtergram, we used the *Hinode* spectropolarimeter (SP) data to study the magnetic field of the sunspot. Unfortunately, no SP data was taken simultaneously with the blue continuum imaging. Instead, we created a composite map of the two closest SP maps taken before and after the filtergram imaging. The maps were taken at 17:58UT on 28 Feb (about 6 hours before the start of the filtergram observation), and at 06:14 on 1 Mar (about 4 hours after the end of the filtergram observation), respectively. The spectral FOV includes the two magnetic-sensitive iron lines Fe I 630.15nm and 630.25nm. The two SP scannings were carried out in normal mode. In this mode, it takes about 45 min to scan the FOV of $76'' \times 82''$ with a polarization accuracy of 0.1%. The observed full Stokes parameters (I, Q, U, V) were processed through a dark field subtraction, a flat fielding, and a thermal drift calibration using *sp-prep.pro*. To extract the magnetic field information, we applied the Milne-Eddington inversion (Yokoyama et al. 2009, in preparation) to the calibrated profiles. As the profiles in umbrae are highly symmetric, the Milne-Eddington inversion works quite well. As a result of the inversion, we obtained maps of the magnetic field strength (B), the field inclination (i), and the field azimuth (ψ). The inclination is an angle between a field line and the local normal, i.e., 0° inclination means a vertical, 90° inclination means a horizontal field line. The field azimuth is measured from 0° - 360° , and 0° azimuth is oriented in the right-to-left (east) direction. The continuum map at around 6303Å was also prepared for the alignment process. The two magnetic maps, taken at the different times, were transformed as if they were observed at 01:30UT on Mar 1 by a coordinate rotation. In this procedure, the magnetic field inclination and azimuth were converted using a planar approximation. Subsequently, the two maps were co-aligned by finding the best cross-correlation displacements and averaged into one map. Then, we enlarged the pixel size of the SP from $0.15'' \times 0.16''$ to $0.054'' \times 0.054''$ in order to co-align

the map with the blue continuum image. Finally, the magnetic strength and inclination maps were boxcar-smoothed with a width of $780\text{km} \times 780\text{km}$ to extract the global structure. We define this composite map as the magnetic field at 01:30UT on Mar 1, and use it for the following analysis. It is worth noting that our composite magnetic map can be used only for retrieving the global magnetic characteristics, because the individual original magnetic maps (6 hours before and 4 hours afterwards) may include local variations, contributed by UDs. Nevertheless, if we study the statistics of the local correlations, we can derive reliable dependencies of the UD's properties on the global magnetic field nature.

As can be seen in Fig. 4.1, the sunspot was almost circular. Two dark core regions with large field strengths >2600 Gauss can be seen in the southern region of the sunspot. Between these two dark cores, a short light bridge is connected to the southern penumbra .

4.3. Automatic Detection Algorithm

For the statistical analysis of the UDs, an automatic detection algorithm is inevitable, because the sunspot of interest includes numerous UDs. Based on previous papers which utilized automated algorithms, such as Sobotka et al. (1997a) and Riethmüller et al. (2008), we constructed a new automatic detection algorithm. Compared to previous work, our algorithm can be kept simpler since the *Hinode* data is free from variable atmospheric seeing conditions.

The algorithm consists of 6 main steps.

1. Identify local peaks where $I(x, y)$ (I : intensity normalized by the averaged quiet region) is equal to the maximum value in its vicinity of ± 2 pixels (± 78 km). (Figure 4.2(b))
2. Construct background image (bg) using the minimum values of the intensity in their vicinity of ± 6 pixels (± 235 km). The obtained image is boxcar-smoothed with a width of 20×20 pixels (782 km). Define the umbra as the region where the intensity of bg is less than 0.4. This umbra region will be analyzed in the following steps. (Figure 4.2(c))
3. Identify UDs at peak positions where $I_{peak}(x, y)/I_{bg}(x, y)$ is larger than 1.3. The total number of UDs in each frame is 124 on average. (Figure 4.2(d))
4. Calculate the size of the UDs. For the size determination, we apply two different methods and take the smaller value of the two. The first method uses the distance from the UD's peak position to the nearest inflection point; the second one uses the distance to the threshold of $0.5*(I_{peak}(x, y) - I_{bg}(x, y)) + I_{bg}(x, y)$, respectively. These calculations are applied to 8 directions spaced at 45° intervals from the peak positions. Finally, we take the median of the 8 values. (Figure 4.2(f))

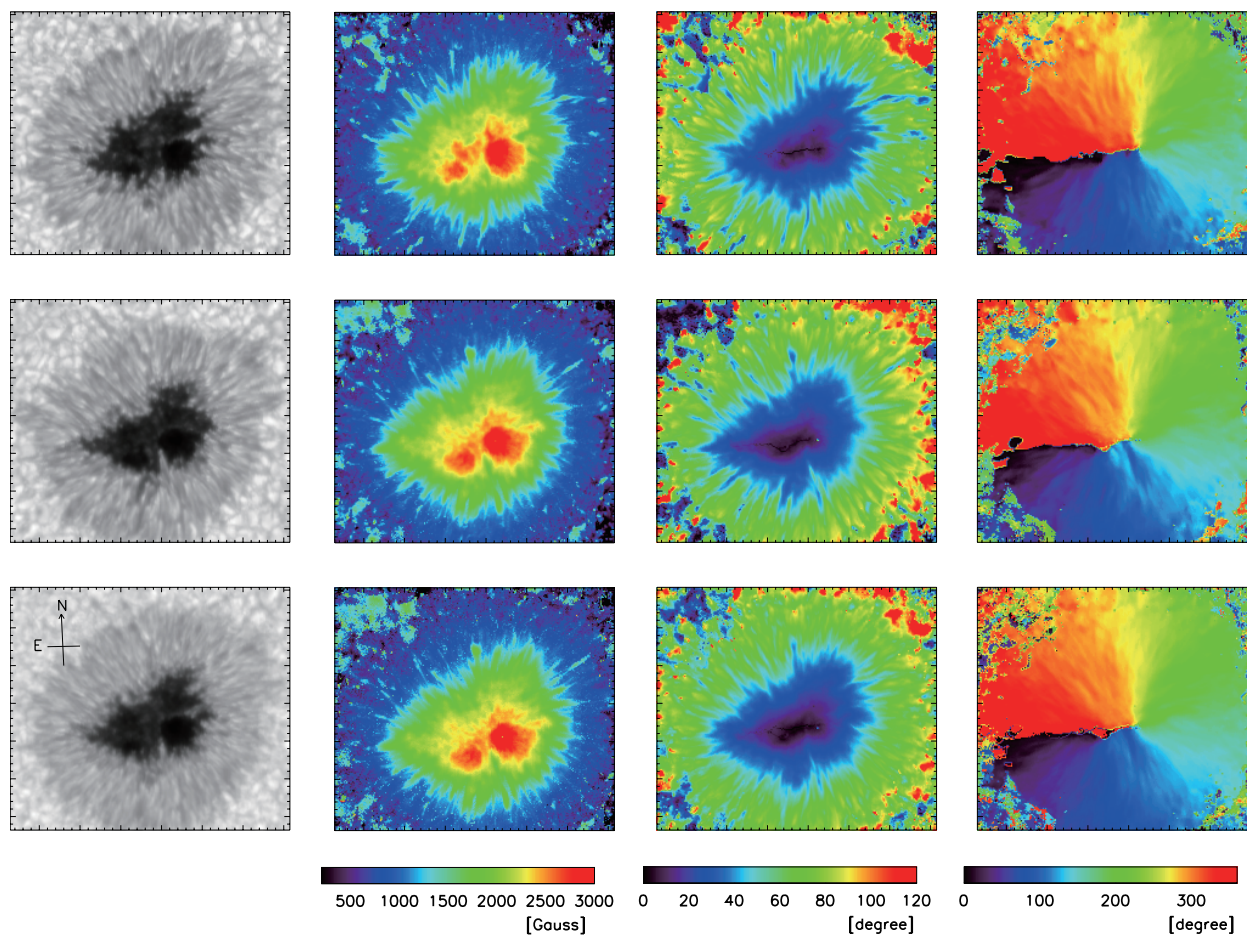


Fig. 4.1.— From left to right: the continuum intensity at $\sim 6303\text{\AA}$, the magnetic field strength, the field inclination, and the field azimuth. From top column to bottom: the SP at 17:58UT on Feb 28 (the images were transformed as if they were observed at 01:30UD on Mar 1, see text), the SP at 06:14UT on Mar 1 (ditto), and the composite map of the two (before smoothing). The tick marks are shown in $1''$ intervals.

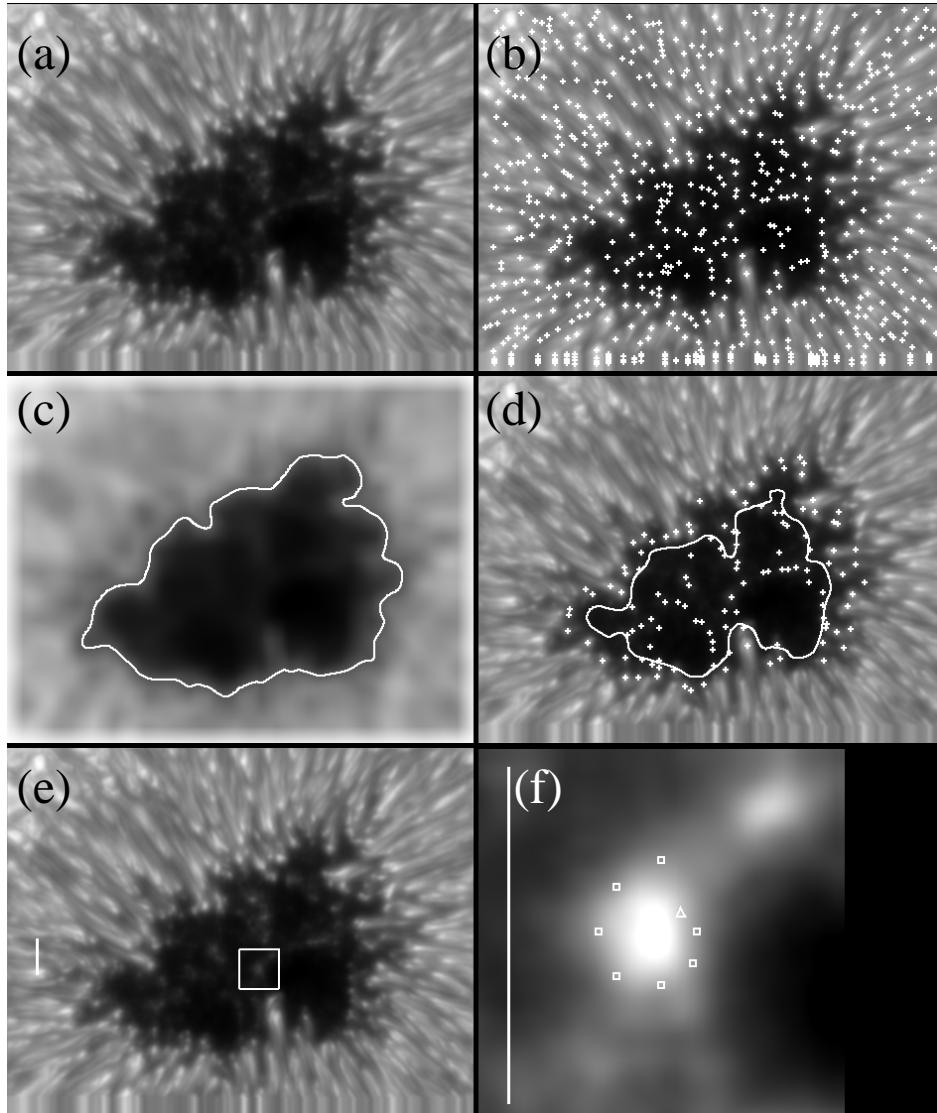


Fig. 4.2.— (a) Hanning filtered image (b) Peak detection (c) Background image. The contour denotes the boundary of the umbra ($I_{bg}=0.4$). (d) UD positions. The contour denotes the boundary of peripheral UDs ($I_{bg} = 0.2$). UDs outside of the contour are peripheral, UDs inside are central. (e) The position of the UD shown in (f). The white line on the left-hand side indicates $2''$ length. (f) An example of the size calculation. The 7 squares (threshold of $I(x, y)=0.5*(I_{peak}(x, y) - I_{bg}(x, y))+I_{bg}(x, y)$) and the triangle (inflection point) indicate the UD's boundary points for 8 directions. Again, the white line on the left-hand side indicates $2''$ length.

5. Once the positions of all UD in every frame are known, the temporal succession of each UD is determined as follows: the succession is confirmed if an UD is found in the next frame (25 seconds later) within ± 2 pixels of its previous position. If no UD is found, the continuation ends at that point. However, if there is another UD within ± 2 pixels in the following one or two frames, the succession is continued. Fission (two UD within ± 2 pixels) and fusion (two UD coalesce into one UD) events are taken into account, though these events are scarce (less than 0.2% of all UD in one frame). This procedure is applied to all UD until all UD disappeared, or the final frame of the data is reached.
6. Classify the UD into two categories, i.e., central and peripheral UD. The boundary between central and peripheral UD is set to the contour line of $I_{bg}=0.2$. Peripheral UD are those who have their origins outside of the $I_{bg}=0.2$ contour. (Figure 4.2(d))

As a result, 2268 UD were detected. Out of these 2268 UD, 825 UD are of central type, and 1443 UD are of peripheral type, respectively. We want to note that 245 UD either already existed before the first observation or lasted longer than the last observation. These 245 UD can not be tracked from the beginning to the end, so we underestimate their lifetimes. Nevertheless, we include these UD in our analysis, because they represent long-life UD.

4.4. Results

We detected the temporal trajectories of 2268 UD in §4.3. Using this information, we calculated 8 parameters which characterize the UD: the lifetime, the average size, the brightness ratio, the velocity amplitude, the velocity orientation, the magnetic field strength, the field inclination, and the field azimuth. These parameters are defined as follows:

- lifetime (T) \cdots (temporal cadence 25 sec) \times (number of frames in which the UD is observed)
- average size (S) \cdots the average of the UD's size over its whole life (the size in each frame is described in §4.3, step [4])
- brightness ratio (R) \cdots the average of I_{peak}/I_{bg} over its whole life
- velocity amplitude ($|V|$) \cdots (the distance between its birth and death location)/(lifetime)
- velocity orientation (v) \cdots the direction from its birth location to its death location measured from 0° - 360° . The 0° direction of the velocity orientation is oriented in the left-to-right (west), i.e., in the opposite direction of the field azimuth.

- magnetic field strength (B) \cdots the magnetic field strength at its origin (note that the magnetic field information is global one composed by two SP maps taken at the different times. See §4.2)
- field inclination (i) \cdots the field inclination at its origin
- field azimuth (ψ) \cdots the field azimuth at its origin

4.4.1. Histogram

Figure 4.3 shows the histograms of the 6 parameters ($T, S, R, |V|, B, i$). The gray and hatched bars indicate the central and the peripheral UDs, respectively. The average values of each parameter are summarized in Table 4.1. Peripheral UDs tend to have brighter intensity, faster proper motion, weaker and more horizontal magnetic field than central UDs. This result is consistent with Sobotka et al. (1997a,b) and Kitai et al. (2007), which supports the validity of our automatic detection method.

4.4.2. Scatter Diagrams

Next, we study the scatter plots of the parameters of the UDs against the magnetic field strength and inclination, as shown in Fig. 4.4. Please refer to Fig. 4.1 for the spatial distributions of the magnetic field components. There is a subtle tendency for the lifetimes to be shorter for strong fields. However, in a coarse view, the lifetimes of UDs are more or less independent of the magnetic field strength and inclination. The sizes of UDs are almost constant around ~ 180 km, with the exception of the dark core region. The dark core region shows field strengths of >2600 Gauss and field inclinations around 20° . The brightness ratio

Table 4.1: Average of UD parameters

	Average of 2268 UDs	Average of 825 central UDs	Average of 1443 peripheral UDs
T [sec]	441	391	469
S [km]	184	178	187
R	1.73	1.51	1.85
$ V $ [km s $^{-1}$]	0.44	0.33	0.50
B [Gauss]	2197	2406	2077
i [degree]	27	17	33

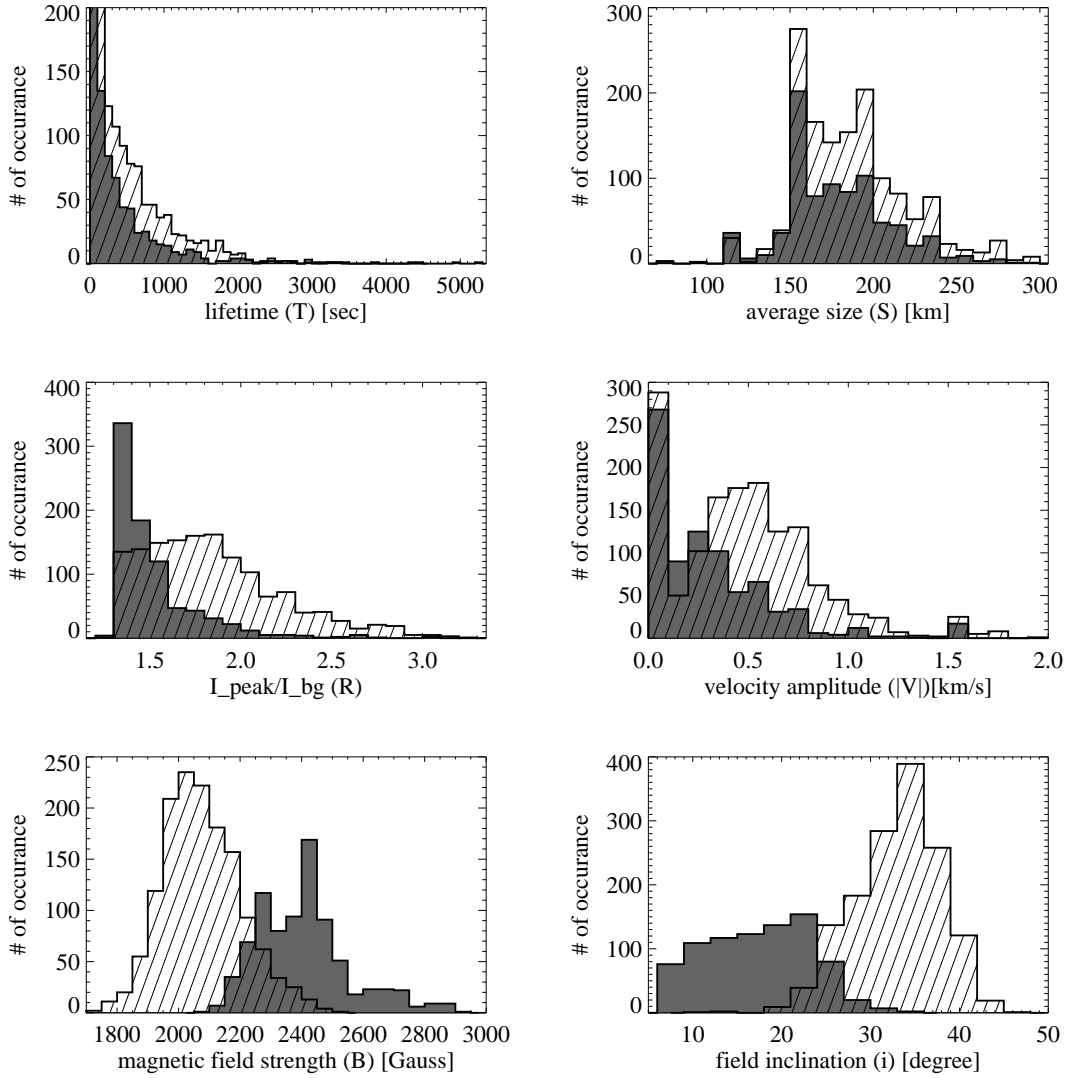


Fig. 4.3.— Histograms for 2268 UD. The gray and hatched regions correspond to the central and peripheral UD, respectively.

I_{peak}/I_{bg} is especially large just inside the penumbra with field inclinations of 25° - 35° , and decreases linearly as the fields get stronger. In the peripheral region with field inclinations of 35° - 40° , the brightness ratio decreases because the background intensity is large. The dependence of the velocity amplitude on the field inclination is more pronounced than on the field strength. The velocity amplitude increases with the field inclination. Figure 4.5 shows 6 scatter diagrams of the velocity orientation of UDs versus the field azimuth for 1762 UDs for different ranges of the field inclination. Here, we ignored 506 UDs which had no detectable movements from their birth to their death, so the velocity orientation could not be determined. Note that the 0° directions of the velocity orientation and the field azimuth have opposite directions. Thus, the motions of UDs toward the center of the sunspot have the same velocity orientation angle as the field azimuth. In the bottom panels of Fig. 4.5, the velocity orientation angles are strongly correlated to the field azimuth. This is because the peripheral UDs generally move inwards. However, this correlation is weaker for UDs with smaller field inclinations (upper panels in Fig. 4.5). The correlation coefficients for the different inclination ranges are: 0.22 (inclination $<15^\circ$), 0.45 (15° - 20°), 0.47 (20° - 25°), 0.63 (25° - 30°), 0.64 (30° - 35°), and 0.75 ($>35^\circ$). The correlation coefficient increases as the field inclination increases. Therefore, we conclude that the velocity orientation of UDs in the large field inclination regions is determined by the field azimuth, while the velocity orientation of UDs in the small field inclination regions is weakly dependent on the field azimuth.

4.4.3. Spatial Distribution

The histograms of the differences of the field strength and the inclination between their death and birth locations are shown in Fig. 4.6. A significant majority (73%) of the peripheral (hatched) and a large amount (56%) of the central UDs (gray) show stronger fields at their death locations than at their birth locations, while only 8.0% of the peripheral and 16% of the central UDs show weaker field strengths. Similar results are found for the field inclination (Fig. 4.6(b)): 73% of the peripheral and 58% of the central UDs show more vertical fields at their death than at their birth, while more inclined fields are detected only for 7.5% of the peripheral and 12% of the central UDs. This means that not only the peripheral UDs, but also the central ones are likely to appear in weaker field regions with more inclined fields and disappear in stronger field region with vertical field orientation. This is a natural consequence for peripheral UDs, because they move inward from the penumbra to the umbra. For central UDs, however, it is less obvious. Further investigations should be performed using temporal variations of magnetic fields.

It is known that dark cores include few UDs (Beckers & Schröter 1968; Kitai et al. 2007). The reason was supposed to be that too strong magnetic field in dark cores prohibit magnetoconvection to be effective. We confirmed that strongly magnetized regions include fewer UDs, as shown also in Fig. 4.7. The occurrence rate is given by the ratio of the number

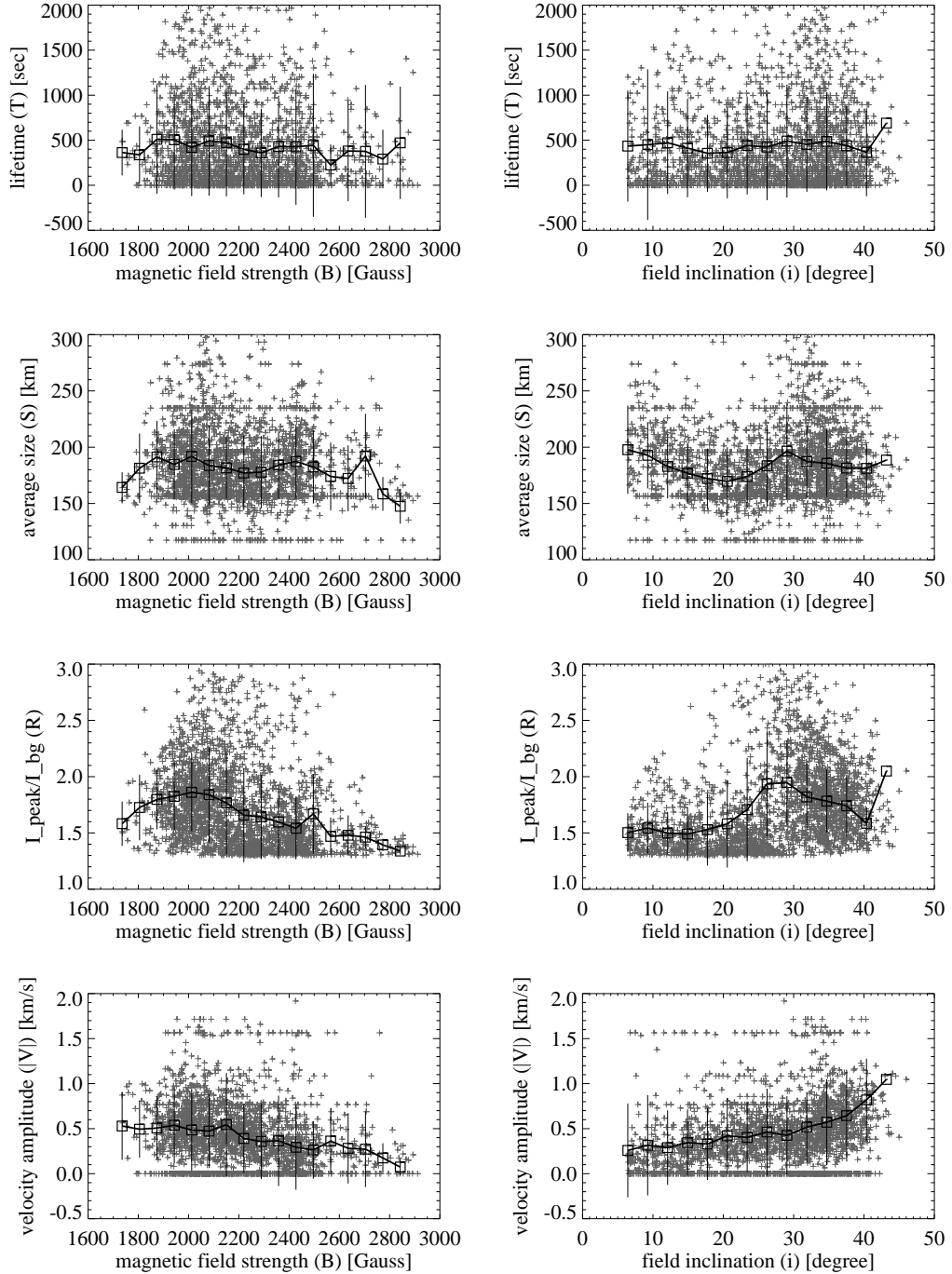


Fig. 4.4.— *Left column:* Scatter plots of the lifetime, the average size, I_{peak}/I_{bg} , and the velocity amplitude versus the magnetic field strength. The average of bins of 70 Gauss is shown in square symbols, and solid lines denote the standard deviation error bars. *Right column:* Scatter plots of the lifetime, the average size, I_{peak}/I_{bg} , and the velocity amplitude versus the field inclination. The average of bins of 3° is shown in square symbols, and solid lines denote the standard deviation error bars.

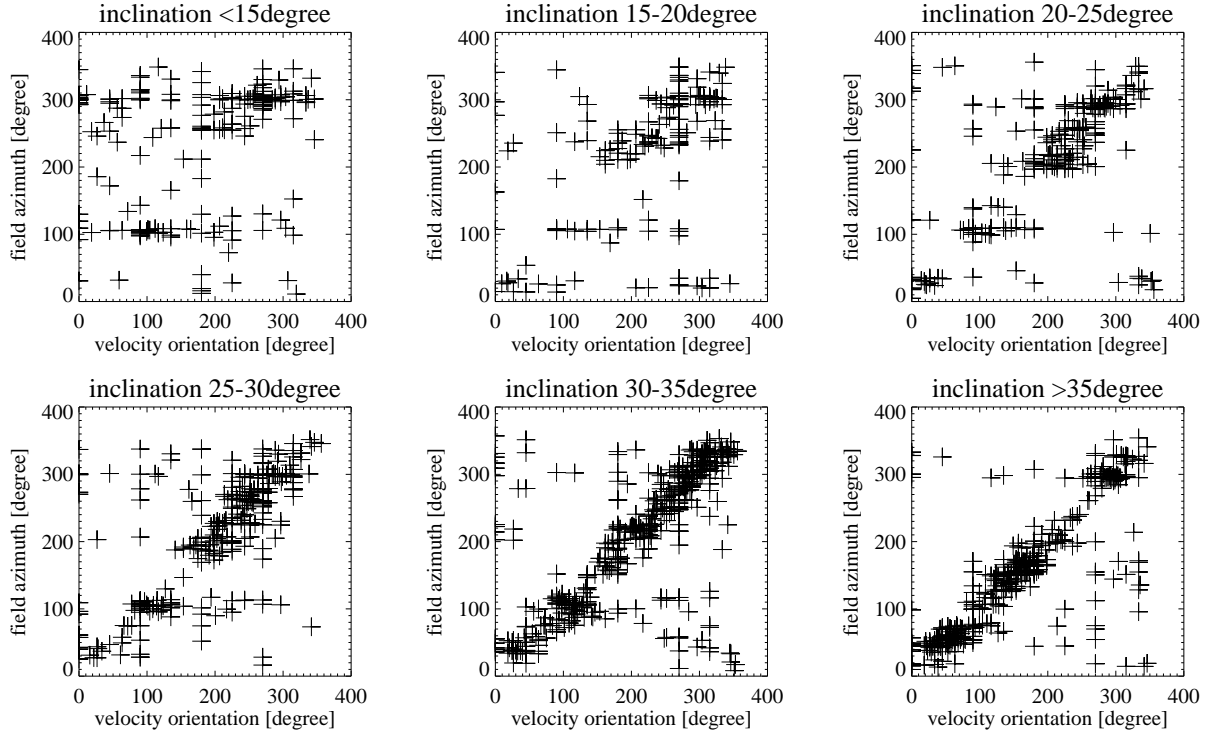


Fig. 4.5.— Scatter plots of the velocity orientation versus the field azimuth for different intervals of the field inclination

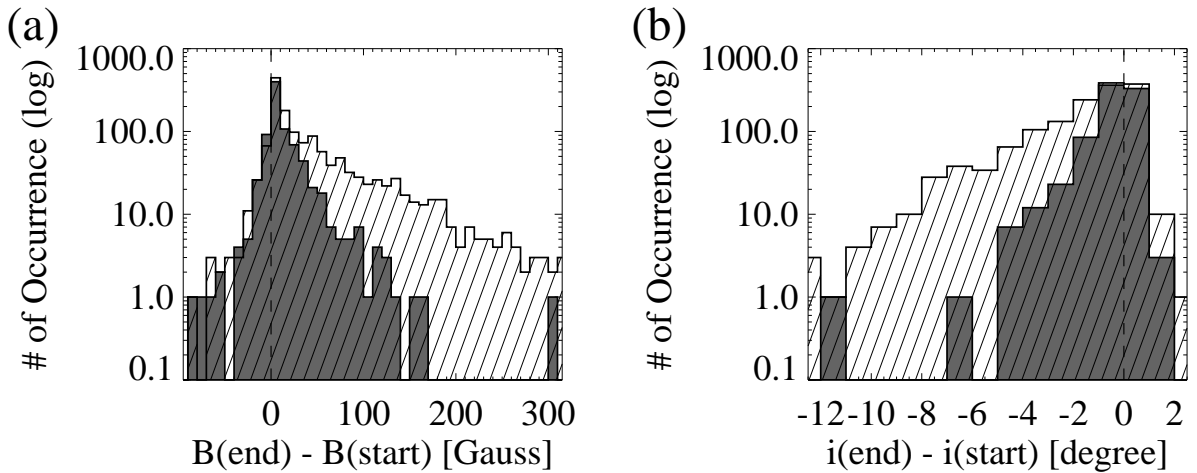


Fig. 4.6.— (a) Histogram of the field strength differences between their death and birth locations (log scale). The gray bars indicate central UDs, the hatched bars indicate peripheral ones. (b) The histogram of the field inclination differences between their death and birth locations (log scale). The gray bars indicate the central UDs, and the hatched bars indicate the peripheral ones.

of UDs within regions of a specific field strength to the area of these regions. The left image in Fig. 4.7 shows the distribution of the appearance positions of all UDs. Many UDs appear in the surrounding areas of the dark cores, which may be an indication of the flux separation (Tao et al. 1998; Weiss et al. 2002).

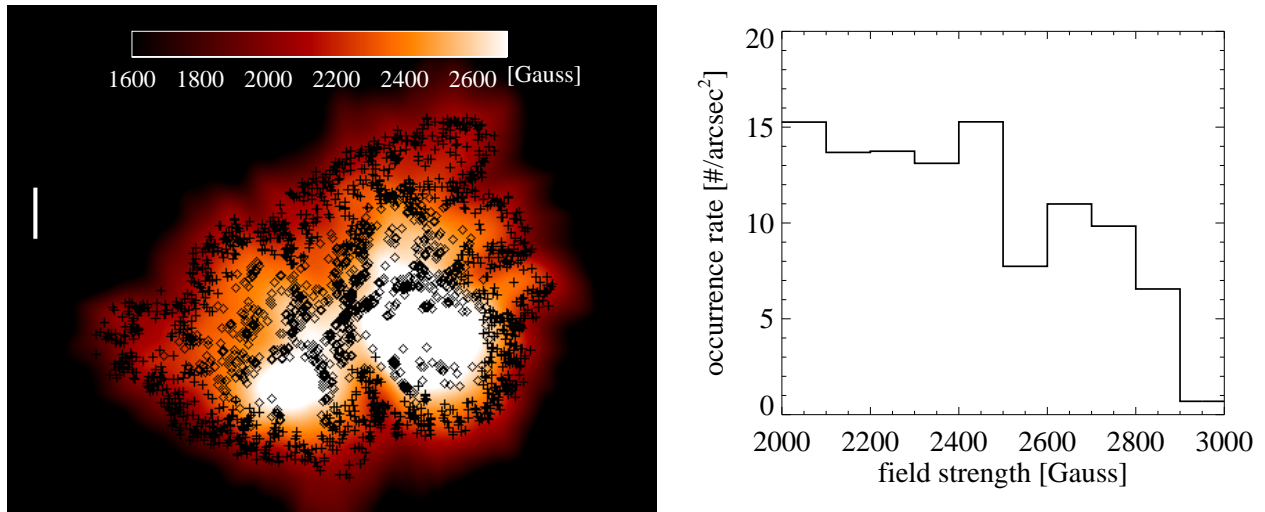


Fig. 4.7.— *Left*: The appearance positions of the central UDs (diamonds) and the peripheral UDs (plus signs), overlaid on the background image of the magnetic field strength. *Right*: The UD’s occurrence rate versus the field strength with field strength bins of 100 Gauss.

4.4.4. Lightcurve

We calculated the characteristic lightcurves by the normalization and averaging method. Only UDs with lifetimes of $T > 120$ s are selected for the analysis in this section. First, the various UD lifetimes are normalized to unity and averaged. The results are shown in Fig. 4.8. The characteristic lightcurves of the central and the peripheral UDs (top panels of Fig. 4.8) have similar shapes as those in Kitai et al. (2007) and Riethmüller et al. (2008). The uniqueness of our analysis lies in the lower 4 plots in Fig. 4.8. The main consequence of different field strength bands is the amplitude of the brightness fluctuations. In the strong field bands, the fluctuations of the brightness ratio get smaller, and the lightcurves show symmetric brightening and darkening. In the weak field bands, the amplitude of the brightness fluctuations is large, and the lightcurves show fast brightening and slow darkening.

Another important properties of the UD’s lightcurves are oscillations. We show the lightcurves of 76 UDs with $T > 1800$ s in Fig. 4.9. The lightcurves are spaced from each other with a constant offset. We arranged the lightcurves depending on their field strengths from top to bottom. The bottommost lightcurve is that of a point in the dark core, which

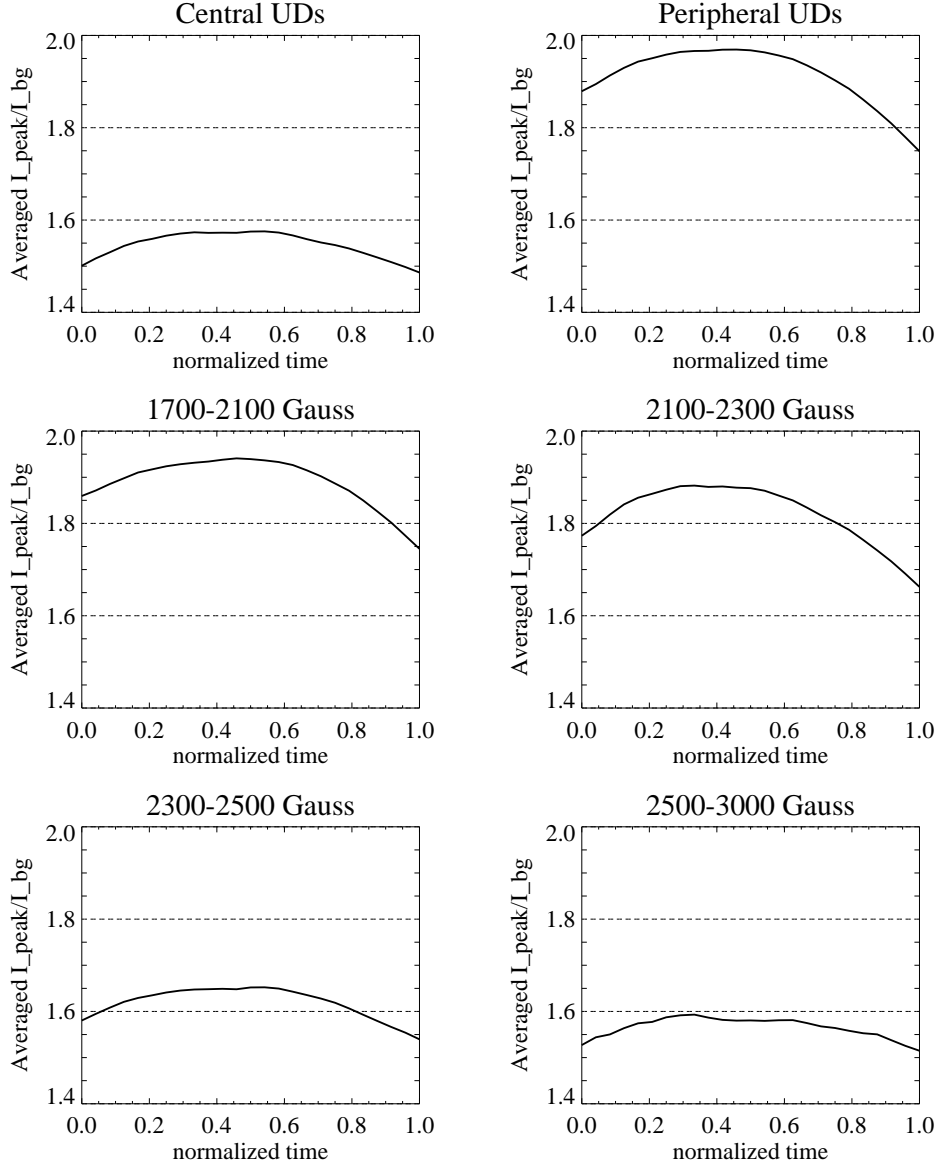


Fig. 4.8.— Averaged lightcurves of the central UD's (*top left*), the peripheral UD's (*top right*), UD's born in 1700-2100 Gauss regions (*middle left*), UD's born in 2100-2300 Gauss regions (*middle right*), UD's born in 2300-2500 Gauss regions (*bottom left*), and UD's born in 2500-3000 Gauss regions (*bottom right*).

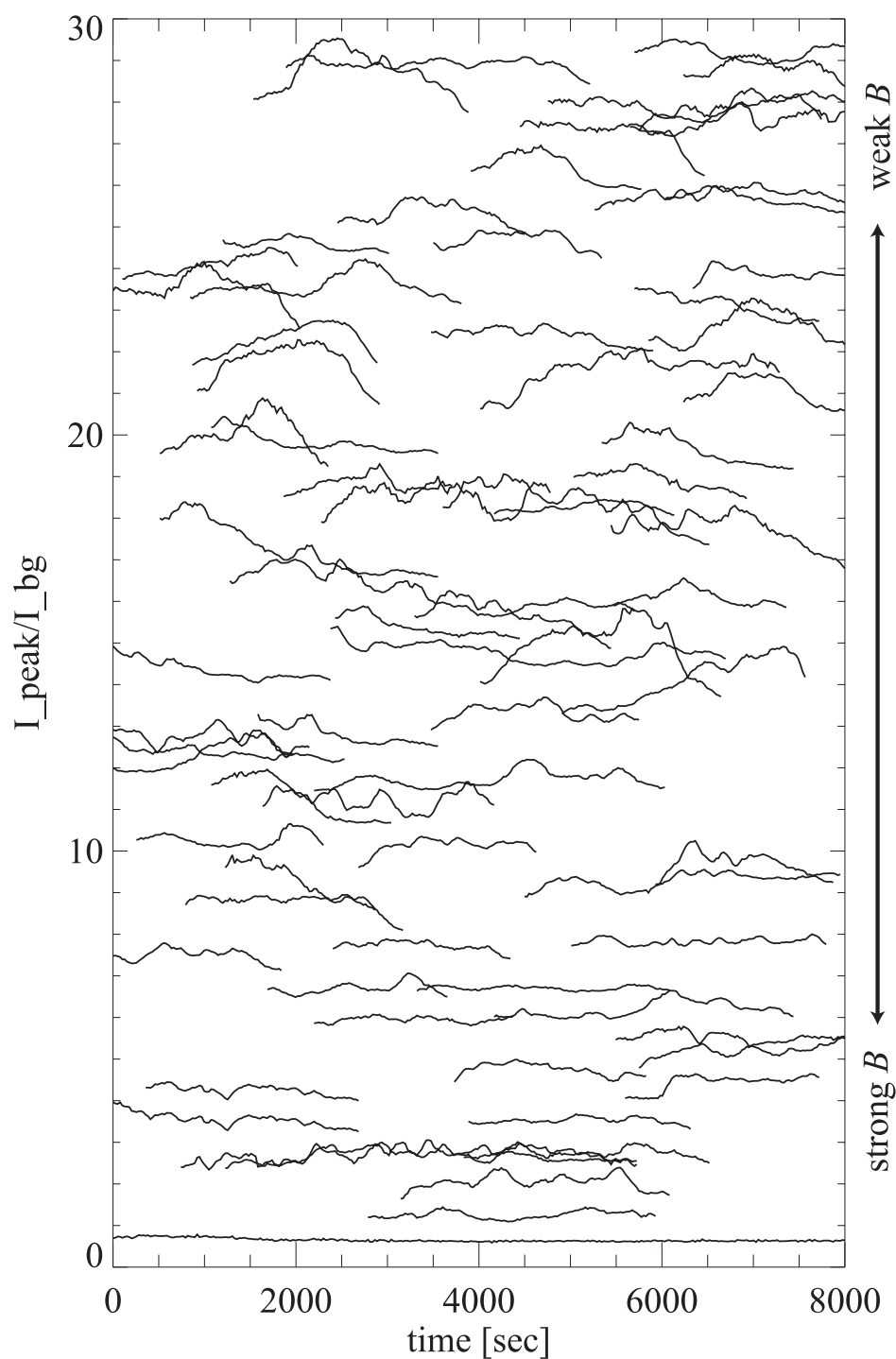


Fig. 4.9.— Lightcurves of 76 UD_s with $T > 1800$ s. The lightcurves are arranged by their field strengths from top to bottom, i.e., the upper curves have the weaker field strength. The lightcurves are spaced by constant vertical offsets. The bottommost lightcurve is that of a point in the dark core.

may represent the error fluctuation level. The lightcurves display oscillatory fluctuations. To find the characteristic frequency of the oscillations, a Fourier transformation analysis was performed. The procedure for the Fourier transformation analysis is as follows: firstly, we differentiate the lightcurves to remove the low frequency components. Secondly, the IDL routine *FFT* (Fast Fourier Transformation) is applied to the differential lightcurves. The power spectrum of the lightcurve is calculated by taking the square of the absolute value of the Fourier transformed function. We normalized the power spectra by the total power of each lightcurve. Figure 4.10 shows the power spectra of 76 lightcurves in color scale. The UDs are arranged by the order of their field strength, i.e., UD 0 corresponds to the strongest field (2738 Gauss) and UD 76 corresponds to the weakest field (1882 Gauss). The lower frequency components around ~ 1 mHz (16 minutes) are dominant for the UDs in the weaker field regions, while ~ 1.5 mHz (10 minutes) frequency components are more important for the UDs in the stronger field regions. However, the distribution of the power spectra is too random to allow conclusions on a common characteristic frequency, including 5 minutes p-mode oscillations (3.3 mHz) and 3 minutes umbra oscillation (5.5 mHz) (Beckers & Schultz 1972). Note that, since the shortest lifetime of the analyzed UDs is 1800 s, the detectable frequency is limited to larger values than 1.1 mHz.

4.5. Discussion

We analyzed in detail the relation between the UD's parameters and the magnetic nature. This pioneering analysis owes greatly to the precise measurement of the magnetic field and the stable high-resolution imaging by the *Hinode* SOT.

The obtained distributions of the lifetime, the average size, and the proper motion of UDs confirm the performance of our automated detection algorithm. The averages of each parameter of the central and the peripheral UDs are listed in Table 4.1. Using 5 parameters, determined by the automated detection algorithm (the lifetime, the average size, the brightness ratio, the velocity amplitude, and the velocity orientation) plus three magnetic field components (the field strength, the field inclination, and the field azimuth), we are able to obtain important correlations. The results can be summarized as follows:

1. Slightly shorter lifetimes were found for the UDs in the strong field regions. The lifetimes show almost no dependence on the field inclination.
2. The average sizes of the UDs are relatively small in the strong field regions, especially in the dark core where the magnetic fields are strongest.
3. The brightness ratios of the UDs and the contrasts of their lightcurves show clear negative correlations with the magnetic field strength.

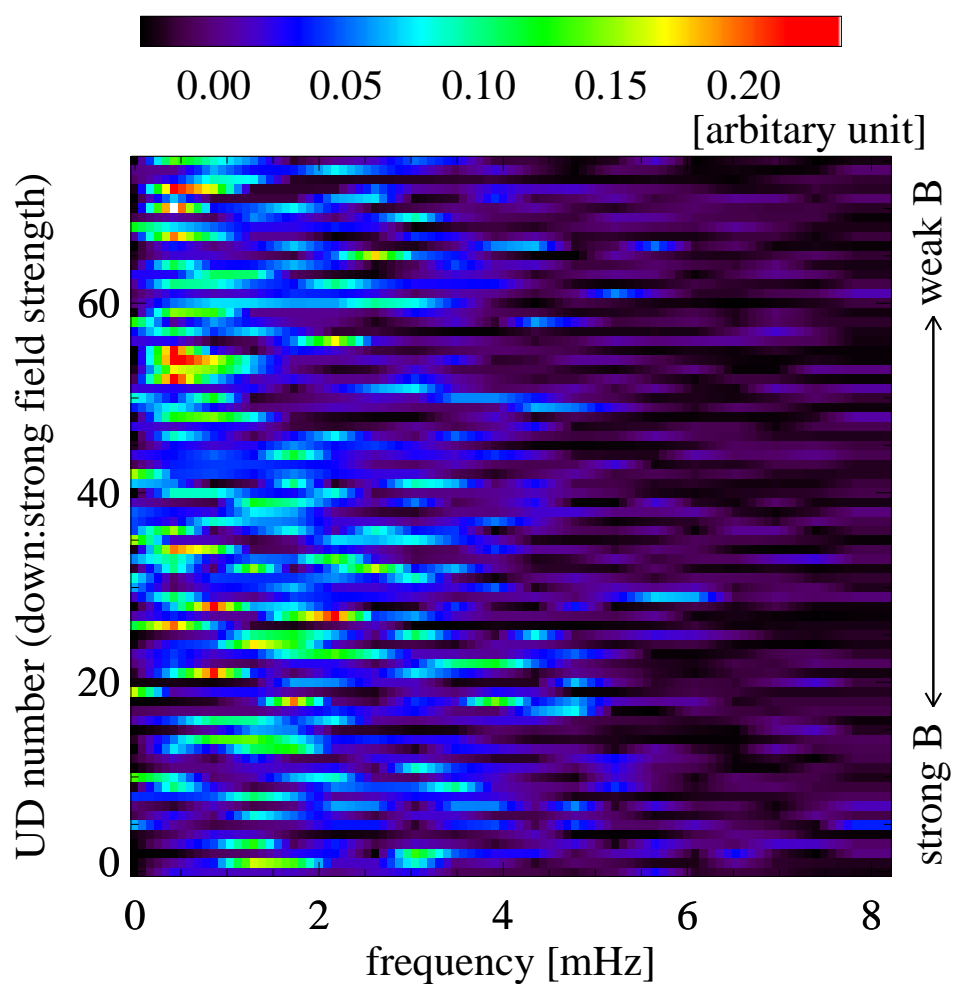


Fig. 4.10.— Distribution of the power spectra of the lightcurves of 76 UD. The horizontal axis indicates the frequency, the vertical axis the arrangement of the 76 UD (lower positions correspond to stronger fields).

4. The velocity amplitudes of the UDs are strongly correlated with the field inclination.
5. The velocity orientations of the UDs in the larger field inclination regions are correlated with field azimuth, while those of the UDs in the smaller field inclination areas only weakly depend on the field azimuth.
6. The UDs tend to have their origins in regions with weaker and more inclined magnetic fields, and to disappear in regions with stronger and vertical magnetic fields.
7. A larger number of UDs appear in the weaker magnetic field regions than in the stronger magnetic field regions.
8. The analysis of the oscillations of the UD's lightcurves reveals that short frequency components around $\sim 1\text{mHz}$ (16 minutes) are dominant for UDs in weaker field regions, while $\sim 1.5\text{mHz}$ (10 minutes) frequency components are prominent for the UDs in the strong field regions.

Our results show that the lifetime, the average size, the occurrence rate, the contrast of the brightness ratio of the lightcurve of the UDs are dependent on the field strength, while the motion of the UDs is strongly related to the magnetic field inclination. The most significant feature is the positive correlation between the field inclination and UD's velocity amplitude. The gappy model (Spruit & Scharmer 2006; Heinemann et al. 2007) can explain the proper motion of the peripheral UDs. When hot gas ascend along the inclined magnetic field, the gas pushes the field apart and creates a gap in the upper region of the field lines (Scharmer et al. 2008). This process causes a reduction of the field strength in the inward side of the gap and makes it easier for gas to be buoyant, which explains the inward migration of peripheral UDs. Another possible mechanism is the moving tube model (Schlichenmaier 2002), in which the inward migration corresponds to a footpoint of a rising flux tube. Both models predict the inward migration for UDs in more inclined fields. The larger correlation coefficient between the field azimuth and the UD's velocity orientation in the larger field inclination region provides further evidence for this behavior. Since the propagation of the gas becomes increasingly difficult with stronger and more vertically aligned fields, the inward migration of the UDs is suppressed in these regions, just as we confirmed in Fig. 4.5

Weiss et al. (2002) explained the UDs as small scale magnetoconvection modified by the existence of strong magnetic fields. They also suggested that vigorous convection should take place in the weakly magnetized area, which may correspond to light bridges. This is a natural consequence of the simple theoretical model of a suppressed eddy motion by strong magnetic fields (Weiss 1981; Blanchflower & Weiss 2002). In fact, we found that UDs in the dark core have smaller sizes than in other regions of the umbra. Ewell (1991) pointed out the possibility that those UDs formed deeper in the umbra might be either intrinsically fainter or smaller. Our result is consistent with his expectations. The statistical analysis of the size

of UDs is strongly affected by the actual definition of their size. A more elaborate study is only possible by a common analysis of both the observed and the simulated (smeared with the point spread function of the instrument) sunspots. The shorter lifetimes we found for UDs in the strong field regions are consistent with the lifetimes of the simulated UDs by Shüssler & Vögler (private communication). The mean lifetime of the reproduced UDs is 34 minutes for 2000 Gauss sunspots, 28 minutes for 2500 Gauss sunspots, and 25 minutes for 3000 Gauss sunspots. Not only the average I_{peak}/I_{bg} , but also the contrasts of the brightness ratio of the lightcurves is smaller for the UDs appearing in the strong field regions. Some 3D MHD simulations, such as Shüssler & Vögler (2006) and Rempel et al. (2008), suggest that the convection creating an UD occupies only a shallow layer of ~ 400 km, in the framework of the monolithic model. The fact that central UDs have smaller sizes and smaller brightness contrasts implies that the intrinsic total heat flux is relatively larger for magnetoconvection in strong fields.

The oscillation analysis of the UD's lightcurves was first carried out by Sobotka et al. (1997b). However, they used ground-based, seeing-affected observation data. Our data is free from such variable atmospheric conditions, which greatly extends the reliability of our analysis. Unfortunately, we could not find any common frequency components that show strong power for the long-living ($T > 40$ min) UDs. The only confirmable signature is that low frequency components around ~ 1 mHz (16 minutes) are dominant for UDs in the weaker field strength regions, while ~ 1.5 mHz (10 minutes) frequency components are prominent for UDs in the strong field regions. The shorter lifetimes for UDs in the strong fields may be related to this result. The interpretation of the lightcurve oscillations of an UD is not straightforward, because they can be caused either by an overlapping with adjacent UDs, by an additional heat flux into the UD, or by the period of the oscillatory magnetoconvection.

Recent 3D MHD simulations have successfully reproduced the basic characters of UDs. The observational properties of UDs found in this study provide a good test for the theory of UDs, and they should be investigated in numerical simulations in future work. This strategy will lead to a more realistic understanding of the structure of sunspots.

REFERENCES

Beckers, J. M., & Schröter, E. H., 1968, 4, 303

Beckers, J. M., & Schultz, R. B., 1972, *Sol. Phys.*, 27, 61

Blanchflower, S., & Weiss, N., 2002, *Phys. Lett. A* 294, 297

Ewell, M. W. 1992, *Sol. Phys.*, 137, 215

Heinemann, T., Nordlund, A., Scharmer, G. B., & Spruit, H. C., 2007, *ApJ*, 669, 1390

- Kitai, R., Watanabe, H., Nakamura, T., et al. 2007, PASJ, 59, 585
- Proctor, M. R. E. & Weiss, N. O. 1982, *Rep. Prog. Phys.*, 45, 1317
- Rempel, M., Shüssler, M., & Knölker, M. 2008, ApJ, in press
- Riethmüller, T. L., Solanki, S. K., Zakharov, V., & Gandorfer, A. 2008, A&A, 233, 243
- Scharmer, G. B., Nordlund, A., & Heinemann, T. 2008, ApJ, 677L, 149S
- Schlichenmaier, R., 2002, *Astron. Nachr.*, 323, 303
- Schüssler, M., & Vögler, A. 2006, ApJ, 641L, 73S
- Sobotka, M., Bonet, A. J., & Vázquez, M. 1994, ApJ, 426, 404S
- Sobotka M., Brandt P. N., & Simon G. W. 1997a, A&A, 328, 682
- Sobotka M., Brandt P. N., & Simon G. W. 1997b, A&A, 328, 689
- Spruit, H. C., & Scharmer, G. B., 2006, A&A, 447, 343
- Tao, L., Weiss, N. O., Brownjohn, D. P., & Proctor, M. R. E., 1998, ApJ, 496, L39
- Tsuneta, S., Ichimoto, K., Katsukawa, Y., et al. 2008, *Sol. Phys.*, 249, 167
- Weiss, N. O. 1981, *Journal of Fluid Mechanics Digital Archive*, 108, 247
- Weiss, N. O., Brownjohn, D. P., Hurlburt, N. E., & Proctor, M. R. E. 1990, MNRAS, 245, 434
- Weiss, N. O., Proctor, M. R. E., Brownjohn, D. P. 2002, MNRAS, 337, 293
-

5. Summary and Future Work

This thesis describes many aspects of umbral dots (UDs) by the best use of the *Hinode* SOT data. The study of the UD's is much more fruitful than we expected, partly because of the collaboration with high-resolution observations and partly because of the contemporary progress in numerical simulations. We can not only address to the basic parameters of a realistic signature of magnetoconvection, but also approach to a substructure of a sunspot.

Table 5 summarizes the basic properties of the UD's, and Table 6 lists the UD's correlations studied in this thesis. Using these valuable information, let us discuss the two biggest questions about UD's and sunspots in more detail. The two questions are; "Do central and peripheral UD's have a different or the same mechanism?" and "Is the sunspot uniform or non-uniform in the subphotosphere?"

"Do central and peripheral UD's have a different or the same mechanism?"

The first motivation to classify UD's into central and peripheral types originates the difference in their proper motions. Peripheral UD's are detached tips from penumbral grains and move towards the center of the umbra. On the other hand, central UD's can not be seen to have any connection to penumbral grains and are motionless. Nevertheless, the central and peripheral UD's have size and lifetime in common, thus indicating a similar mechanism should occur. The fact that no histograms of the parameters of the UD's show double-peaked distributions is also supporting evidence for their similarity.

The gappy model, which was originally introduced for the theory of the penumbra by Spruit & Scharmer (2006), explains that the both types of UD's have the same convective mechanism. The discrepancy in their motions, they explain, is caused only by the bent angle of the magnetic field (see Fig. 3 in Spruit & Scharmer 2006). When a hot gas ascend along an inclined magnetic field, the gas illuminates the upper area of the field anisotropically and causes a reduction of the magnetic field. Then, because of the reduction of the magnetic field, the gas is pushed up in the inward side of the inclined magnetic field. This process occurs progressively, and is observed as the inward migration of the UD's. The linear dependence of the UD's velocity amplitude on the field inclination (Fig. 4.4), and the strong correlation between UD's velocity orientation and the field azimuth in more horizontal fields (Fig. 4.5), are strongly supporting their idea. The moving flux tube model (Schlichenmaier et al. 1997a,b) is another mechanism that accounts for the inward migration of the peripheral UD's by the buoyancy of the inclined magnetic field. However, since the moving tube model can not suffice the heat flux needed to compensate the observed radiation of the penumbra, it is considered less promising.

Table 5.1. UD basic properties summary

Parameter	Type	Results	Reference
Size	*C,*P	280km (median)	§2.4.1
Lifetime	C,P	14.5minutes (median)	§2.4.2
	light bridge	19.5minutes (median)	§2.4.2
Proper motion	C	null and random	§2.4.3
	P	0.9km s ⁻¹ and decelerate toward umbra	§2.4.3
Temperature	C	4600K (average)	§2.4.4
	P	5460K (average)	§2.4.4
Field strength	C,P	-17Gauss (average)	§3.4.4
Field inclination	C,P	more horizontal 0.6° (average)	§3.4.4
Doppler velocity	C,P	-28m s ⁻¹ (average)	§3.4.4
Fusion & Fission	C	only a few cases were observed	§2.4.7
	*C: central	*P: peripheral	

Table 5.2. UD correlations

Parameter	v.s.	Positive or Negative	Reference
Peak brightness	Background brightness	positive	§2.4.6
	Amplitude of blue shift	positive	§3.4.3
Field strength	Length of lifetime	negative (low reliable)	§4.4.2
	Size	negative (low reliable)	§4.4.2
	Brightness ratio	negative	§4.4.2
	Fluctuating range of lightcurve	negative	§4.4.2
	Occurrence rate	negative	§4.4.3
	Power of long-period oscillation	negative (low reliable)	§4.4.4
Field inclination	Velocity amplitude	positive	§4.4.2
Field azimuth	Velocity orientation	consistent only for *P	§4.4.2
		*P: peripheral	

”Is the sunspot uniform or non-uniform in the subphotosphere?”

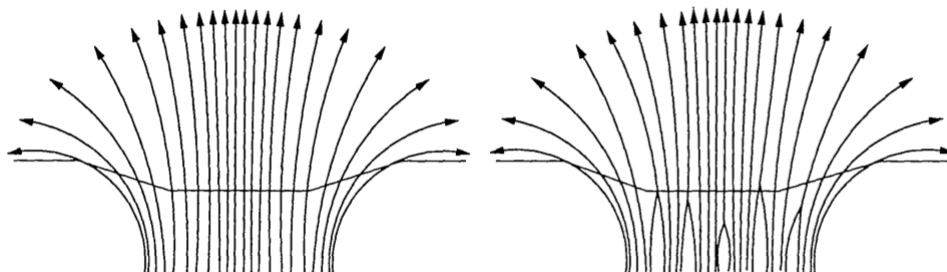


Fig. 5.1.— Cartoon of a monolithic (left) and a spaghetti (right) models of a sunspot. The thin solid line represents the optical depth unity layer. (Fig.1 in del Toro Iniesta 2001)

Although sunspots are studied intensively by many authors, the hidden substructure of them is still controversial. The ideas can be roughly divided into two groups: “the spaghetti model” represented by Parker (1979), and “the monolithic model” represented by Weiss (1997) (Fig. 5.1). The spaghetti model considers a sunspot as a cluster of thin flux tubes, and it assumes UDs as field-free gas that are finding their way by pushing aside the surrounding flux tubes. In the monolithic model, a sunspot consists of a single monolithic flux tube, and an UD is a manifestation of magnetoconvection. It is difficult for observation to find a definite proof of one of these model, because the differences are hidden in the unobservable subsurface. The dependence investigation of the UDs on their magnetic field, as we done in §4, for sunspots in their various evolutionary phases may provide conclusive evidence, since a growing or a disappearing sunspot might be more like the spaghetti sunspot. The quickest way is to compare the MHD simulation and the real observation, and polish up the simulation. This kind of approach is waited to be done.

Future work: Remaining observational approaches to UDs

The *Hinode* satellite has brought us uncountable fantastic data. Then, have we already gone as far as we can in the observations of sunspot fine structures? The answer is “No”. One of the observational frontier is the temporal variation of magnetic fields. A measurement of magnetic fields in a short temporal cadence is completely difficult, because of long exposure times and requisite rotations of a waveplate. We are planning to perform an optimized observation for the measurement of magnetic fields in a short temporal cadence. Our plan is to scan a narrow region ($4''$ in scan direction \times $20''$ in slit direction) repeatedly with less than 3 minutes intervals. This observational proposal is already submitted and soon accepted by the *Hinode* core team. A mature sunspot is being waited for appearing on the solar surface. Hopefully we will get the data by summer in this year.

We do not restrict ourselves in analyzing only the *Hinode* data. We just started a collaborative study of the velocity field around UDs using the IBIS data. IBIS is an abbreviation for “Interferometric Bidimensional Spectrometer”, which is one of the most powerful equipment in Dunn Solar Telescope in Sunspot, New Mexico. IBIS can perform a multi-point wavelength scanning of Fe I 709.0nm. As Fe I 709.0nm line has the Lande factor $g = 0$, the spectral shape is suitable for velocity analysis. Moreover, we can derive the temporal variation of accompanying velocity field of UDs.

Also, UD’s characteristics variation depending on various sunspots is very interesting subject. We already started a preliminary work on this project. UDs in pores typically have larger size than the UDs in sunspot. UDs in disintegrating sunspots have smaller size than the UDs in mature sunspots. These results are very preliminary and we are eager to progress this analysis.

REFERENCES

- Spruit, H. C., Scharmer, G. B., 2006, A&A, 447, 343
- Schlichenmaier, R., Jahn, K., & Schmidt, H. U., 1998a, ApJ, 493, L121
- Schlichenmaier, R., Jahn, K., & Schmidt, H. U., 1998b, A&A, 337, 897
- Schüssler, M., & Vögler, A. 2006, ApJ, 641L, 73S
- Parker, E. N., 1979, ApJ, 234, 333
- Weiss, N. O., 1997, ASPC, 118, 21
- del Toro Iniesta, J. C., 2001, ASPC, 248, 35
-